High-Nuclearity Metal–Cyanide Clusters: Synthesis, Magnetic Properties, and Inclusion Behavior of Open-Cage Species Incorporating [(tach)M(CN)$_3$] (M = Cr, Fe, Co) Complexes

Jenny Y. Yang, Matthew P. Shores, Jennifer J. Sokol, and Jeffrey R. Long*

Department of Chemistry, University of California, Berkeley, California 94720-1460

The use of 1,3,5-triaminocyclohexane (tach) as a capping ligand in generating metal–cyanide cage clusters with accessible cavities is demonstrated. The precursor complexes [(tach)M(CN)$_3$] (M = Cr, Fe, Co) are synthesized by methods similar to those employed in preparing the analogous 1,4,7-triazacyclononane (tacn) complexes. Along with [(tach)Fe(CN)$_3$]$^{1-}$, the latter two species are found to adopt low-spin electron configurations. Assembly reactions between [(tach)M(CN)$_3$] (M = Fe, Co) and [M′(H$_2$O)$_6$]$^{2+}$ (M′ = Ni, Co) in aqueous solution afford the clusters [(tach)$_4$(H$_2$O)$_{12}$Ni$_4$Co$_4$(CN)$_{12}$]$^{8+}$, [(tach)$_4$(H$_2$O)$_{12}$Co$_8$(CN)$_{12}$]$^{8+}$, and [(tach)$_4$(H$_2$O)$_{12}$Ni$_4$Fe$_4$(CN)$_{12}$]$^{8+}$, each possessing a cubic arrangement of eight metal ions linked through edge-spanning cyanide bridges. This geometry is stabilized by hydrogen-bonding interactions between tach and water ligands through an intervening solvate water molecule or bromide counteranion. The magnetic behavior of the Ni$_4$Fe$_4$ cluster indicates weak ferromagnetic coupling ($J = 5.5$ cm^{-1}) between the Ni^{II} and Fe^{III} centers, leading to an $S = 6$ ground state. Solutions containing [(tach)Fe(CN)$_3$] and a large excess of [Ni(H$_2$O)$_6$]$^{2+}$ instead yield a trigonal pyramidal [(tach)(H$_2$O)$_{15}$Ni$_3$Fe(CN)$_3$]$^{6+}$ cluster, in which even weaker ferromagnetic coupling ($J = 1.2$ cm^{-1}) gives rise to an $S = {}^7/_2$ ground state. Paralleling reactions previously performed with [(Me$_3$tacn)Cr(CN)$_3$], [(tach)Cr(CN)$_3$] reacts with [Ni(H$_2$O)$_6$]$^{2+}$ in aqueous solution to produce [(tach)$_8$Cr$_8$Ni$_6$(CN)$_{24}$]$^{12+}$, featuring a structure based on a cube of Cr^{III} ions with each face centered by a square planar [Ni(CN)$_4$]$^{2-}$ unit. The metal–cyanide cage differs somewhat from that of the analogous Me$_3$tacn-ligated cluster, however, in that it is distorted via compression along a body diagonal of the cube. Additionally, the compact tach capping ligands do not hinder access to the sizable interior cavity of the molecule, permitting host–guest chemistry. Mass spectrometry experiments indicate a 1:1 association of the intact cluster with tetrahydrofuran (THF) in aqueous solution, and a crystal structure shows the THF molecule to be suspended in the middle of the cluster cavity. Addition of THF to an aqueous solution containing [(tach)Co(CN)$_3$] and [Cu(H$_2$O)$_6$]$^{2+}$ templates the formation of a closely related cluster, [(tach)$_8$(H$_2$O)$_6$Cu$_6$Co$_8$(CN)$_{24}$⊃THF]$^{12+}$, in which paramagnetic Cu^{II} ions with square pyramidal coordination are situated on the face-centering sites. Reactions intended to produce the cubic [(tach)$_4$(H$_2$O)$_{12}$Co$_8$(CN)$_{12}$]$^{8+}$ cluster frequently led to an isomeric two-dimensional framework, [(tach)(H$_2$O)$_3$Co$_2$(CN)$_3$]$^{2+}$, exhibiting *mer* rather than *fac* stereochemistry at the [Co(H$_2$O)$_3$]$^{2+}$ subunits. Attempts to assemble larger edge-bridged cubic clusters by reacting [(tach)Cr(CN)$_3$] with [Ni(cyclam)]$^{2+}$ (cyclam = 1,4,8,11-tetraazacyclotetradecane) complexes instead generated extended one- or two-dimensional solids. The magnetic properties of one of these solids, two-dimensional [(tach)$_2$(cyclam)$_3$Ni$_3$Cr$_2$(CN)$_6$]I$_2$, suggest metamagnetic behavior, with ferromagnetic intralayer coupling and weak antiferromagnetic interactions between layers.

Introduction

An extraordinary variety of chemical and physical properties have been realized in solids composed of extended metal−cyanide frameworks.[1] Many of these compounds are microporous, retaining their framework structure upon dehydration and functioning as molecular sieves.[2] Related phases incorporating guest alkali metal cations have proven effective as ion-exchange materials.[3] Recently, however,

---

* Author to whom correspondence should be addressed. E-mail: jlong@cchem.berkeley.edu.

(1) Dunbar, K. R.; Heintz, R. A. *Prog. Inorg. Chem.* **1997**, *45*, 283 and references therein.

particular attention has been devoted to manipulating the magnetic properties of such compounds. Here, the ease with which various metal ions are substituted into a given structure type has enabled the design of materials displaying a range of unique properties, including photo-[4] and electrochemically induced[5] magnetism, magnetic pole inversion,[6] and magnetooptical effects.[7]

Efforts to extend this vast chemistry into the molecular regime have only just begun. Already, the alkali metal ion exchange chemistry of certain Prussian blue-type solids has been mimicked in molecular metal−cyanide cages.[8] Of particular interest to many, however, is the prospect of controlling the magnetic properties in metal−cyanide clusters.[9,10] Toward that end, the preference of cyanide for a linear bridging geometry lends a degree of predictability to the synthesis of new structures. Combined with the well-understood nature of pairwise magnetic exchange interactions across a cyanide bridge,[11] this then raises the possibility of

assembling molecules with extremely high-spin ground states. Ultimately, by also incorporating magnetic anisotropy in the form of a negative axial zero-field splitting, D, one might produce new single-molecule magnets[12] exhibiting higher blocking temperatures.

Our approach to synthesizing high-nuclearity metal−cyanide clusters has largely involved the use of capping ligands such as 1,4,7-triazacyclononane (tacn) as a means of directing structure. In condensation reactions between a cyano complex and an aquo complex, these capping ligands can preempt growth of an extended framework, leading to formation of a discrete cyano-bridged molecule. For example, the following reaction in aqueous solution affords an octanuclear cluster:[9a]

$$4[(tacn)Co(CN)_3] + 4[(tacn)Co(H_2O)_3]^{3+} \rightarrow$$
$$[(tacn)_8Co_8(CN)_{12}]^{12+} \quad (1)$$
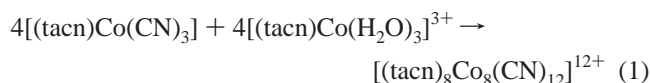
Representing a single cage unit excised from a Prussian blue-type framework,[13] the structure of the product consists of a molecular cube, with Co^{III} ions positioned at the corners and a cyanide ligand spanning each edge. Larger clusters with a greater potential spin can be realized by performing related reactions in which only one of the components features a capping ligand, in this case, the nitrogen-methylated derivative of tacn, *N*,*N*′,*N*″-trimethyl-1,4,7-tri-

(2) (a) Seifer, G. B. *Russ. J. Inorg. Chem.* **1959**, *4*, 841. (b) Seifer, G. B. *Russ. J. Inorg. Chem.* **1962**, *7*, 899. (c) Beall, G. W.; Milligan, W. O.; Petrich, J. A.; Swanson, B. I. *Inorg. Chem.* **1978**, *17*, 2978. (d) Herren, F.; Fischer, P.; Ludi, A.; Hälg, W. *Inorg. Chem.* **1980**, *19*, 956. (e) Cartaud, P.; Cointot, A.; Renaud, A. *J. Chem. Soc., Faraday Trans.* **1981**, *77*, 1561. (f) Williams, D.; Kouvetakis, J.; O'Keeffe, M. *Inorg. Chem.* **1998**, *37*, 4617. (g) Shores, M. P.; Beauvais, L. G.; Long, J. R. *J. Am. Chem. Soc.* **1999**, *121*, 775. (h) Shores, M. P.; Beauvais, L. G.; Long, J. R. *Inorg. Chem.* **1999**, *38*, 1648. (i) Bennett, M. V.; Beauvais, L. G.; Shores, M. P.; Long, J. R. *J. Am. Chem. Soc.* **2001**, *123*, 8022.

(3) (a) Barton, G. B.; Hepworth, J. L.; McClanahan, E. D., Jr.; Moore, R. L.; van Tuyl, H. H. *Ind. Eng. Chem.* **1958**, *50*, 212. (b) Seifer, G. B.; Makarova, Z. A. *Russ. J. Inorg. Chem.* **1964**, *9*, 1498. (c) Krtil, J. *Radiochim. Acta* **1966**, *7*, 30. (d) Kawamura, S.; Kuraku, H.; Kurotaki, K. *Anal. Chim. Acta* **1970**, *49*, 317. (e) Dvorák, P. *Z. Naturforsch.* **1971**, *B26*, 277. (f) Vlasselaer, S.; d'Olieslager, W.; d'Hont, M. *J. Inorg. Nucl. Chem.* **1976**, *38*, 327. (g) Nielsen, D.; Dresow, B.; Heinrich, H. C. *Z. Naturforsch.* **1987**, *B42*, 1451. (h) Loos-Neskovic, C.; Fedoroff, M.; Mecherri, M. O. *Analyst* **1990**, *115*, 981. (i) Bennett, M. V.; Shores, M. P.; Beauvais, L. G.; Long, J. R. *J. Am. Chem. Soc.* **2000**, *122*, 6664.

(4) (a) Sato, O.; Iyoda, T.; Fujishima, A.; Hashimoto, K. *Science* **1996**, *272*, 704. (b) Gu, Z.-Z.; Sato, O.; Iyoda, T.; Hashimoto, K.; Fujishima, A. *Chem. Mater.* **1997**, *9*, 1092. (c) Bleuzen, A.; Lomenech, C.; Escax, V.; Villain, F.; Varret, F.; Cartier dit Moulin, C.; Verdaguer, M. *J. Am. Chem. Soc.* **2000**, *122*, 6648. (d) Pejakovic, D. A.; Manson, J.; Miller, J. S.; Epstein, A. J. *Phys. Rev. Lett.* **2000**, *85*, 1994. (e) Gu, Z.-Z.; Einaga, Y.; Sato, O.; Fujishama, A.; Hashimoto, K. *J. Solid State Chem.* **2001**, *159*, 336.

(5) Sato, O.; Iyoda, T.; Fujishima, A.; Hashimoto, K. *Science* **1996**, *271*, 49.

(6) (a) Ohkoshi, S.; Yorozu, S.; Sato, O.; Iyoda, T.; Fujishima, A.; Hashimoto, K. *Appl. Phys. Lett.* **1997**, *70*, 1040. (b) Ohkoshi, S.; Iyoda, T. *Phys. Rev. B* **1997**, *56*, 11642. Ohkoshi, S.; Abe, Y.; Fujishima, A.; Hashimoto, K. *Phys. Rev. Lett.* **1999**, *82*, 1285. (d) Ohkoshi, S.; Hashimoto, K. *J. Am. Chem. Soc.* **1999**, *121*, 10591.

(7) (a) Mizuno, M.; Ohkoshi, S.; Hashimoto, K. *Adv. Mater.* **2000**, *12*, 1955. (b) Ohkoshi, S.; Mizuno, M.; Hung, G.; Hashimoto, K. *J. Phys. Chem. B* **2000**, *104*, 9365.

(8) (a) Klausmeyer, K. K.; Rauchfuss, T. B.; Wilson, S. R. *Angew. Chem., Int. Ed.* **1998**, *37*, 1694. (b) Klausmeyer, K. K.; Wilson, S. R.; Rauchfuss, T. B. *J. Am. Chem. Soc.* **1999**, *121*, 2705. (c) Contakes, S. M.; Kuhlman, M. L.; Ramesh, M.; Wilson, S. R.; Rauchfuss, T. B. *Proc. Natl. Acad. Sci. U.S.A.* **2002**, *99*, 4889.

(9) (a) Heinrich, J. L.; Berseth, P. A.; Long, J. R. *Chem. Commun.* **1998**, 1231. (b) Berseth, P. A.; Sokol, J. J.; Shores, M. P.; Heinrich, J. L.; Long, J. R. *J. Am. Chem. Soc.* **2000**, *122*, 9655. (c) Sokol, J. J.; Shores, M. P.; Long, J. R. *Angew. Chem., Int. Ed.* **2001**, *40*, 236. (d) Heinrich, J. L.; Sokol, J. J.; Hee, A. G.; Long, J. R. *J. Solid State Chem.* **2001**, *159*, 293. (e) Shores, M. P.; Sokol, J. J.; Long, J. R. *J. Am. Chem. Soc.* **2002**, *124*, 2279. (f) Sokol, J. J.; Shores, M. P.; Long, J. R. *Inorg. Chem.* **2002**, *41*, 3052. (g) Sokol, J. J.; Hee, A. G.; Long, J. R. *J. Am. Chem. Soc.* **2002**, *124*, 7656.

(10) (a) Mallah, T.; Auberger, C.; Verdaguer, M.; Veillet, P. *J. Chem. Soc., Chem. Commun.* **1995**, 61. (b) Sculiler, A.; Mallah, T.; Verdaguer, M.; Nivorzkhin, A.; Tholence, J.-L.; Veillet, P. *New J. Chem.* **1996**, *20*, 1. (c) Vahrenkamp, H.; Geiss, A.; Richardson, G. N. *J. Chem. Soc., Dalton Trans.* **1997**, 3643 and references therein. (d) Rajendiran, T. M.; Mathonière, C.; Golhen, S.; Ouahab, L.; Kahn, O. *Inorg. Chem.* **1998**, *37*, 2651. (e) Oshio, H.; Tamada, O.; Onodera, H.; Ito, T.; Ikoma, T.; Tero-Kubota, S. *Inorg. Chem.* **1999**, *38*, 5686. (f) Zhao, L.; Matthews, C. J.; Thompson, L. K.; Heath, S. L. *Chem. Commun.* **2000**, 265. (g) Zhong, Z. J.; Seino, H.; Mizobe, Y.; Hidai, M.; Fujishima, A.; Ohkoshi, S.; Hashimoto, K. *J. Am. Chem. Soc.* **2000**, *122*, 2952. (h) Larionova, J.; Gross, M.; Pilkington, M.; Andres, H.; Stoeckli-Evans, H.; Güdel, H. U.; Decurtins, S. *Angew. Chem., Int. Ed.* **2000**, *39*, 1605. (i) Parker, R. J.; Spiccia, L.; Berry, K. J.; Fallon, G. D.; Moubaraki, B.; Murray, K. S. *Chem. Commun.* **2001**, 333. (j) Depperman, E. C.; Bodnar, S. H.; Vostrikova, K. E.; Schultz, D. A.; Kirk, M. L. *J. Am. Chem. Soc.* **2001**, *123*, 3133. (k) Smith, J. A.; Galán-Mascarós, J.-R.; Clérac, R.; Sun, J.-S.; Ouyang, X.; Dunbar, K. R. *Polyhedron* **2001**, *20*, 1727. (l) Marvilliers, A.; Hortholary, C.; Rogez, G.; Audière, J.-P.; Rivière, E.; Boquera, J. C.; Paulsen, C.; Villar, V.; Mallah, T. *J. Solid State Chem.* **2001**, *159*, 302. (m) Podgajny, R.; Desplanches, C.; Sieklucka, B.; Sessoli, R.; Villar, V.; Paulsen, C.; Wernsdorfer, W.; Dromzée, Y.; Verdaguer, M. *Inorg. Chem.* **2002**, *41*, 1323.

(11) (a) Entley, W. R.; Treadway, C. R.; Girolami, G. S. *Mol. Cryst. Liq. Cryst.* **1995**, *273*, 153. (b) Weihe, H.; Güdel, H. U. *Comments Inorg. Chem.* **2000**, *22*, 75.

(12) (a) Sessoli, R.; Tsai, H.-L.; Schake, A. R.; Wang, J. B.; Folting, K.; Gatteschi, D.; Christou, G.; Hendrickson, D. N. *J. Am. Chem. Soc.* **1993**, *115*, 1804. (b) Sessoli, R.; Gatteschi, D.; Caneschi, A.; Novak, M. A. *Nature* **1993**, *365*, 141. (c) Barra, A.-L.; Debrunner, P.; Gatteschi, D.; Schulz, C. E.; Sessoli, R. *Europhys. Lett.* **1996**, *35*, 133. (d) Aubin, S. M. J.; Wemple, M. W.; Adams, D. M.; Tsai, H.-L.; Christou, G.; Hendrickson, D. N. *J. Am. Chem. Soc.* **1996**, *118*, 7746. (e) Castro, S. L.; Sun, Z.; Grant, C. M.; Bollinger, J. C.; Hendrickson, D. N.; Christou, G. *J. Am. Chem. Soc.* **1998**, *120*, 2365. (f) Goodwin, J. C.; Sessoli, R.; Gatteschi, D.; Wernsdorfer, W.; Powell, A. K.; Heath, S. L. *J. Chem. Soc., Dalton Trans.* **2000**, 1835. (g) Boskovic, C.; Brechin, E. K.; Streib, W. E.; Folting, K.; Bollinger, J. C.; Hendrickson, D. N.; Christou, G. *J. Am. Chem. Soc.* **2002**, *124*, 3725.

(13) Buser, H. J.; Schwarzenbach, D.; Petter, W.; Ludi, A. *Inorg. Chem.* **1977**, *16*, 2704.

azacyclononane (Me$_3$tacn):[9b]

$$8[(Me_3tacn)Cr(CN)_3] + 6[Ni(H_2O)_6]^{2+} \rightarrow$$
$$[(Me_3tacn)_8Cr_8Ni_6(CN)_{24}]^{12+} \quad (2)$$
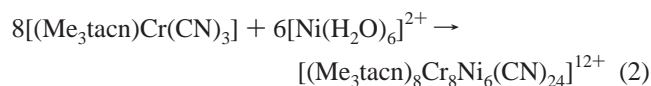
Here, cluster assembly is followed by a thermally induced cyanide linkage isomerization to give a face-centered cubic species, with Cr^{III} ions situated at the corners of a cube and square planar [Ni(CN)$_4$]$^{2−}$ units spanning each face. Analogous to the situation for metal−cyanide framework solids, the possibility of substituting different transition metal ions into these geometries provides a method for varying both spin state and magnetic anisotropy.[9e,g]

An intriguing aspect of the aforementioned clusters is the presence of an internal cavity defined by the rigid, tightly connected metal−cyanide cage. Both [(tacn)$_8$Co$_8$(CN)$_{12}$]$^{12+}$ and [(Me$_3$tacn)$_8$Cr$_8$Ni$_6$(CN)$_{24}$]$^{12+}$ possess a hydrophobic interior, which, as crystallized from aqueous solution, is devoid of guest molecules or ions. Exhibiting a nearly spherical cavity with a volume of 284 Å^3 (based on van der Waals radii),[2g] the latter species presents a particularly attractive candidate for exploring host−guest chemistry. Twelve distorted square Cr$_2$Ni$_2$(CN)$_4$ windows provide entry points through which a guest molecule might enter the cavity. Unfortunately, however, access is severely restricted by the methyl substituents of the Me$_3$tacn ligands, which project directly over these openings. To obtain variants of the cluster with less restricted access to the cavity, we have therefore pursued the possibility of utilizing *cis,cis*-1,3,5-triaminocyclohexane (tach)—a symmetric, tridentate capping ligand offering considerably less steric hindrance—in place of Me$_3$tacn.

tacn   tach
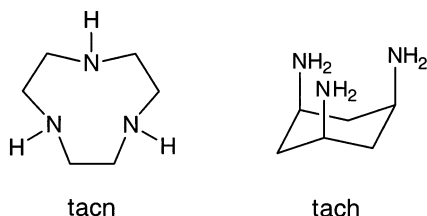
Herein, we report the synthesis and cluster assembly reaction chemistry of the complexes [(tach)M(CN)$_3$] (M = Cr, Fe, Co), along with the magnetic and preliminary inclusion properties of the ensuing metal−cyanide cage molecules.

Experimental Section

Preparation of Compounds. Preparations of compounds **1**−**5** were carried out under a pure dinitrogen atmosphere; all other preparations were conducted in air. The compounds tach·3HBr,[14] Fe(CF$_3$SO$_3$)$_2$·1.6MeCN,[15] [Ni(cyclam)I$_2$],[16] and [Cu(cyclam)](NO$_3$)$_2$·4H$_2$O[17] were synthesized as described previously. Water was distilled and deionized with a Milli-Q filtering system. Diethyl ether and tetrahydrofuran were passed through alumina and degassed prior to use. Acetonitrile was distilled over CaH$_2$ and degassed prior to use. All other reagents were obtained from commercial vendors and used without further purification.

[(tach)Cr(CO)$_3$] (1). Solid tach·3HBr (2.5 g, 6.7 mmol) was added to a solution of sodium methoxide (1.1 g, 0.020 mol) in 60 mL of THF. The mixture was heated at reflux for 1 h and then filtered. The resulting filtrate was concentrated to a volume of 3 mL under reduced pressure and then added to 45 mL of mesitylene. Solid Cr(CO)$_6$ (1.5 g, 6.7 mmol) was added and the solution was heated at reflux under a dinitrogen atmosphere. In the first hour of heating, the solution was swirled occasionally to prevent solid Cr-(CO)$_6$ from collecting on the sides of the flask. After 4 h of heating, the reaction was cooled to −25 °C. The ensuing bright yellow precipitate was collected by filtration, washed with successive aliquots of benzene (10 mL) and ether (20 mL), and dried in a stream of dinitrogen to yield 1.6 g (90%) of product. This compound is somewhat sensitive to light and air. IR: ν_{CO} 1885, 1696 cm^{-1}. Anal. Calcd for C$_9$H$_{15}$CrN$_3$O$_6$: C, 40.76; H, 5.70; N, 15.85. Found: C, 40.66; H, 5.78, N, 15.51.

[(tach)CrBr$_3$] (2). Under a pure dinitrogen atmosphere, a mixture of 150 mL of chloroform and liquid bromine (16 g, 0.10 mol) was added to solid **1** (1.6 g, 6.0 mmol). The mixture was heated and stirred at reflux for 10 h, cooled to room temperature, and stirred for an additional 1 h. The resulting solid was collected by filtration, washed with successive aliquots of chloroform (2 × 15 mL) and ether (30 mL), and dried under reduced pressure to give 2.5 g (99%) of product as a hygroscopic blue-green solid. Absorption spectrum (DMSO): λ_{max} (ϵ_M) 397 (53), 542 (82) nm. Anal. Calcd for C$_9$H$_{19}$-CrN$_6$O$_2$ (**2**·2H$_2$O): C, 15.77; H, 4.19; N, 9.20. Found: C, 16.34; H, 3.67; N, 8.87.

[(tach)Cr(CN)$_3$]·H$_2$O (3). A solution of **2** (0.53 g, 1.2 mmol) in 6 mL of DMSO was stirred and heated at 50 °C for 45 min to produce a dark magenta solution. Anhydrous NaCN (1.8 g, 37 mmol) was added to the solution, and the mixture was stirred and heated at 50 °C for 4 days, prompting formation of a yellow precipitate. After addition of 10 mL of ethanol to aid product precipitation, a first crop of solid product was collected by filtration of the hot reaction mixture. The red filtrate was then reduced to dryness in vacuo to give an orange solid. The solid was stirred for 2 min under 30 mL of cold water, and a second crop of product was collected by filtration. The solids were combined, washed with 15 mL of cold water, and dried in air to give 0.25 g (72%) of yellow product. Absorption spectrum (H$_2$O): λ_{max} (ϵ_M) 332 (62), 417 (71) nm. IR: ν_{CN} 2132 cm^{-1}. μ_{eff} (295 K): 3.89 μ_B. Anal. Calcd for C$_9$H$_{17}$CrN$_6$O: C, 38.99; H, 6.18; N, 30.31. Found: C, 38.77; H, 6.17; N, 30.15. Yellow block-shaped crystals of **3** suitable for X-ray analysis were grown by slow evaporation of a concentrated aqueous solution of the product.

[(tach)Fe(CF$_3$SO$_3$)$_2$(MeCN)$_{0.4}$] (4). Solid tach·3HBr (1.0 g, 2.7 mmol) was added to a solution of sodium methoxide (0.50 g, 9.3 mmol) in 40 mL of THF. The mixture was heated at reflux for 1 h and then filtered, and the resulting pale yellow filtrate was reduced to dryness in vacuo. A solution of this solid in 4 mL of acetonitrile was then added dropwise to a solution of Fe(CF$_3$SO$_3$)$_2$·1.6MeCN (1.1 g, 2.7 mmol) in 20 mL of acetonitrile. The ensuing purple solution was stirred at room temperature for 4 days, whereupon a small amount of brown precipitate was separated by filtration. The filtrate was concentrated to a volume of 3 mL under reduced pressure, and 250 mL of ether was added to induce formation of a

(14) Bowen, T.; Planalp, R. P.; Brechbiel, M. W. *Bioorg. Med. Chem. Lett.* **1996**, *6*, 807.
(15) Blakesley, D. W.; Payne, S. C.; Hagen, K. S. *Inorg. Chem.* **2000**, *39*, 1979.
(16) (a) Bosnich, B.; Tobe, M. L.; Webb, G. A. *Inorg. Chem.* **1965**, *4*, 1109. (b) Iwamoto, E.; Imai, K.; Yamamoto, K. *Inorg. Chem.* **1984**, *23*, 986.
(17) Clay, R. M.; Steele, W. V. *Inorg. Chem.* **1980**, *19*, 2414.

light tan precipitate. The solid was collected by filtration, washed with 25 mL of ether, and dried under vacuum to afford 1.2 g (94%) of product. IR: ν_{CN} 2314, 2286, ν_{SO} 1215 cm^{-1}. Anal. Calcd for $C_{8.8}H_{16.2}F_6FeN_{3.4}O_6S_2$: C, 21.16; H, 3.27; N, 9.53. Found: C, 21.34; H, 3.06; N, 9.26. Colorless block-shaped crystals of [(tach)Fe(CF$_3$SO$_3$)$_2$(MeCN)] (3·0.6MeCN) suitable for X-ray analysis were grown by diffusing ether into a concentrated acetonitrile solution of the product.

Na[(tach)Fe(CN)$_3$]·MeOH (5). Anhydrous NaCN (0.50 g, 0.010 mol) was added to a pale orange solution of **4** (1.4 g, 2.7 mmol) in 120 mL of dimethylformamide (DMF). The solution was stirred at room temperature for 5 days, prompting formation of an orange precipitate. The solid was collected by filtration, washed with successive aliquots of DMF (20 mL) and ether (20 mL), and dried under vacuum. Diffusion of ether into a solution of this solid in 50 mL of methanol gave orange rod-shaped crystals of **5·2MeOH** suitable for X-ray analysis. Upon decanting the mother liquor, the crystals were washed with 30 mL of ether and dried under dinitrogen to yield 0.63 g (73%) of dull orange product. Absorption spectrum (MeOH): λ_{max} (ϵ_M) 280 (931, sh), 346 (178), 446 (147) nm. IR: ν_{CN} 2052, 2014 cm^{-1}. μ_{eff} (295 K): 1.30 μ_B. Mössbauer spectra (δ, ΔE_Q, Γ): 0.175, 0.44, 0.25 mm/s at 295 K and 0.239, 0.46, 0.28 mm/s at 90 K. Anal. Calcd for $C_{10}H_{19}FeN_6NaO$: C, 37.75; H, 6.02; N, 26.42. Found: C, 37.50; H, 6.13; N, 26.23.

[(tach)Fe(CN)$_3$]·H$_2$O (6). A solution of **5** (0.14 g, 0.44 mmol) in 8 mL of methanol was added to a solution of iodine (0.18 g, 0.71 mmol) in 12 mL of methanol. The resulting brown mixture was stirred in air for 2 h to give a yellow precipitate, which was collected by filtration. The solid was washed with successive aliquots of methanol (20 mL) and water (50 mL), affording an initial crop of product. The yellow solution obtained from the aqueous wash was concentrated to a volume of 5 mL to give a second crop of product in the form of orange block-shaped crystals suitable for X-ray analysis. The combined solids were dried in air to yield 0.12 g (97%). Absorption spectrum (H$_2$O): λ_{max} (ϵ_M) 259 (1984), 312 (565), 373 (424) nm. IR: ν_{CN} 2121 cm^{-1}. μ_{eff} (295 K): 2.63 μ_B. Mössbauer spectra (δ, ΔE_Q, Γ): 0.021, 0.59, 0.25 mm/s at 295 K and 0.084, 0.72, 0.29 mm/s at 90 K. Anal. Calcd for $C_9H_{17}FeN_6O$: C, 38.45; H, 6.10; N, 29.89. Found: C, 38.44; H, 6.24; N, 29.78.

[(tach)Co(CN)$_3$]·H$_2$O (7·H$_2$O). The preparation of this compound closely followed a previously reported procedure.[18] IR: ν_{CN} 2127 cm^{-1}. Anal. Calcd for $C_9H_{17}CoN_6O$: C, 38.04; H, 6.03; N, 29.57. Found: C, 38.16; H, 5.97; N, 29.46. Yellow block-shaped crystals of **7** suitable for X-ray analysis were grown by gradually cooling a saturated solution of the product in DMSO.

[(tach)$_4$(H$_2$O)$_{12}$Ni$_4$Co$_4$(CN)$_{12}$]Br$_8$·23H$_2$O (8·5H$_2$O). A solution of **7·H$_2$O** (30 mg, 0.11 mmol) and NiBr$_2$·6H$_2$O (0.16 g, 0.48 mmol) in 20 mL of water was heated at reflux and concentrated to a volume of 2 mL. The solution was allowed to cool to room temperature and filtered. Further concentration to a volume of ca. 0.5 mL via evaporation in air produced green block-shaped crystals of **8** suitable for X-ray analysis. The crystals were collected by filtration, washed with successive aliquots of cold water (0.5 mL) and Et$_2$O (5 mL), and dried in air to give 22 mg (45%) of product. IR: ν_{CN} 2187 cm^{-1}. μ_{eff} (295 K): 6.66 μ_B. Anal. Calcd for $C_{36}H_{130}Br_8Co_4N_{24}Ni_4O_{35}$: C, 16.83; H, 5.10; N, 13.08. Found: C, 16.63; H, 5.12; N, 12.82. The water content of this compound was confirmed by thermogravimetric analysis. Green block-shaped crystals of **8·4H$_2$O** were obtained by slow evaporation of a concentrated aqueous

solution of the product from an analogous reaction carried out without applying any heat.

[(tach)$_4$(H$_2$O)$_{12}$Co$_8$(CN)$_{12}$]Br$_8$·8H$_2$O (9). Solid **7** (50 mg, 0.09 mmol) was mixed with a 10 mL aqueous solution of CoBr$_2$ (40 mg, 0.09 mmol) to produce a red-orange solution containing some undissolved **7**. The mixture was twice heated to dryness and then redissolved in water. Pink block-shaped crystals of **9** suitable for X-ray analysis formed when the resulting mixture was allowed to evaporate slowly. Isolation of this compound without some contamination by **15** could not be achieved. IR: ν_{CN} 2174 cm^{-1}.

[(tach)$_4$(H$_2$O)$_{12}$Ni$_4$Fe$_4$(CN)$_{12}$]Br$_8$·18H$_2$O (10). A saturated solution of **6** (80 mg, 0.28 mmol) and NiBr$_2$·6H$_2$O (0.50 g, 1.5 mmol) in 15 mL of water was stirred at room temperature and allowed to evaporate slowly. The mixture was filtered when the volume was reduced to 5 mL, removing a trace amount of brown solid. Diffusion of THF vapor into the resulting green filtrate afforded green block-shaped crystals and a yellow powder. The yellow solid was separated by decanting the suspension obtained upon sonication of the mixture, and the remaining green crystals were washed with THF (4 × 5 mL) and briefly dried in air to yield 81 mg (47%) of product. IR: ν_{CN} 2175 cm^{-1}. μ_{eff} (295 K): 7.88 μ_B. Anal. Calcd for $C_{36}H_{120}Br_8Fe_4N_{24}Ni_4O_{30}$: C, 17.53; H, 4.90; N, 13.63. Found: C, 17.40; H, 4.82; N, 13.73. The water content of this compound was confirmed by thermogravimetric analysis. Rectangular block-shaped crystals of **10·2H$_2$O** suitable for X-ray analysis were grown by slow evaporation of the green filtrate.

[(tach)(H$_2$O)$_{15}$Ni$_3$Fe(CN)$_3$]Br$_6$·2H$_2$O (11·H$_2$O). A solution of **6** (85 mg, 0.30 mmol) and NiBr$_2$·6H$_2$O (0.50 g, 1.5 mmol) in 35 mL of water was stirred at room temperature for 3 h. A small amount of undissolved **6** was removed by filtration to give a pale green solution. The solution was concentrated to a volume of 2 mL under a flow of dinitrogen and then allowed to stand for 2 days. The resulting precipitate (consisting primarily of green square plate-shaped crystals of **10**) was separated by filtration to give a dark green filtrate. Green rod-shaped crystals of **11** suitable for X-ray analysis formed when this solution was allowed to stand for 2 weeks. The crystals were collected by filtration, washed with 15 mL of ether, and dried under a stream of dinitrogen to afford 100 mg (27%) of product. IR: ν_{CN} 2179, 2170 cm^{-1}. μ_{eff} (295 K): 6.37 μ_B. Anal. Calcd for $C_9H_{49}Br_6FeN_6Ni_3O_{17}$: C, 8.82; H, 4.04; N, 6.86. Found: C, 8.73; H, 4.03; N, 6.46. The water content of this extremely hygroscopic compound was confirmed by thermogravimetric analysis.

[(tach)$_8$Cr$_8$Ni$_6$(CN)$_{24}$]Br$_{12}$·30H$_2$O (12). A solution of **3** (79 mg, 0.29 mmol) and NiBr$_2$·6H$_2$O (80 mg, 0.25 mmol) in 8 mL of water was stirred at room temperature for 1 day. A small amount of colorless solid was separated by filtration, and the orange filtrate was concentrated to a volume of 0.5 mL under a flow of dinitrogen. The resulting orange solid was collected by filtration, washed with 30 mL of acetonitrile, and dried in air to give 76 mg (54%) of pale orange product. Absorption spectrum (H$_2$O): λ_{max} (ϵ_M) 268 (63650), 287 (23720), 335 (8925, sh), 452 (495) nm. IR: ν_{CN} 2178 cm^{-1}. FT-ICR ES$^+$-MS (H$_2$O): m/z 1048.14 ([**12** − 3Br − 30H$_2$O]$^{3+}$), 766.38 ([**12** − 4Br − 30H$_2$O]$^{4+}$), 596.92 ([**12** − 5Br − 30H$_2$O]$^{5+}$), 484.29 ([**12** − 6Br − 30H$_2$O]$^{6+}$). μ_{eff} (295 K): 11.32 μ_B. Anal. Calcd for $C_{72}H_{150}Br_{12}Cr_8N_{48}Ni_6O_{30}$: C, 22.03; H, 4.62; N, 17.13. Found: C, 21.95; H, 4.60; N, 17.13. The water content of this compound was confirmed by thermogravimetric analysis; however, it should be noted that water content can vary depending on humidity. Yellow-orange block-shaped crystals of **12·6H$_2$O** suitable for X-ray analysis were obtained by slow evaporation of the filtered reaction mixture.

(18) (a) Umehara, M.; Ishii, M.; Nomura, T.; Muramatsu, I.; Nakahara, M. *Nippon Kagaku Kaishi*, **1980**, 657. (b) Ishii, M.; Umehara, M.; Nakahara, M. *Bull. Chem. Soc. Jpn.*, **1987**, *60*, 125.

Table 1. Crystallographic Data[a] for **3**, **4**·0.6MeCN, **5**·2MeOH, **6**, **7**, and **8**·4H$_2$O

	3	**4·0.6MeCN**	**5·2MeOH**	**6**	**7**	**8·4H$_2$O**
formula	C$_9$H$_{17}$CrN$_6$O	C$_{10}$H$_{18}$F$_6$FeN$_4$O$_6$S$_2$	C$_{12}$H$_{27}$FeN$_6$NaO$_3$	C$_9$H$_{17}$FeN$_6$O	C$_9$H$_{15}$CoN$_6$	C$_{36}$H$_{128}$Br$_8$Co$_4$N$_{24}$Ni$_4$O$_{34}$
formula wt	227.29	524.25	382.24	281.14	266.20	2551.46
T, K	155	153	173	162	166	159
space group	$Pca2_1$	$P2_1/n$	$C2/c$	$Pbca$	$Pnma$	$P\bar{4}2m$
Z	4	4	8	8	4	1
a, Å	11.8998(5)	8.247(3)	22.471(2)	11.584(1)	16.230(11)	13.9193(4)
b, Å	8.3910(4)	18.282(7)	9.6988(7)	12.613(1)	9.237(6)	
c, Å	12.7800(6)	13.049(5)	16.427(1)	16.841(2)	7.609(5)	12.8152(4)
β, deg		94.780(8)	102.003(1)			
V, Å^3	1282.0(1)	1961(1)	3501.8(4)	2460.6(4)	1141(1)	2482.9(1)
d_{calc}, g/cm^3	1.443	1.776	1.450	1.518	1.550	1.706
R_1 (wR_2),[b] %	1.90 (4.51)	3.17 (7.40)	10.89 (29.93)	3.94 (8.38)	2.66 (5.45)	4.60 (13.30)

[a] Obtained with graphite-monochromated Mo Kα (λ = 0.71073 Å) radiation for **3**, [(tach)Cr(CN)$_3$]·H$_2$O; **4**·0.6MeCN, [(tach)Fe(CF$_3$SO$_3$)$_2$(MeCN)]; **5**·2MeOH, Na[(tach)Fe(CN)$_3$]·3MeOH; **6**, [(tach)Fe(CN)$_3$]·H$_2$O; **7**, [(tach)Co(CN)$_3$]; and **8**·4H$_2$O, [(tach)$_4$(H$_2$O)$_{12}$Ni$_4$Co$_4$(CN)$_{12}$]Br$_8$·22H$_2$O. [b] $R_1 = \Sigma||F_o| - |F_c||/\Sigma|F_o|$, w$R_2 = \{\Sigma[w(F_o{}^2 - F_c{}^2)^2]/\Sigma[w(F_o{}^2)^2]\}^{1/2}$.

[(tach)$_8$Cr$_8$Ni$_6$(CN)$_{24}$⊃THF]Br$_{12}$·30H$_2$O (13). Diffusion of THF vapor into a solution of **12**·13H$_2$O (40 mg, 9.6 μmol) in 0.5 mL of water produced orange rod-shaped crystals of **13**·11H$_2$O suitable for X-ray analysis. The crystals were collected by filtration, washed with 5 mL of THF, and dried in air to give 33 mg (86%) of product. IR: ν_{CN} 2171 cm^{-1}. FT-ICR ES$^+$-MS (H$_2$O): m/z 1072.18 ([**13** − 3Br − 30H$_2$O]$^{3+}$), 784.41 ([**13** − 4Br − 30H$_2$O]$^{4+}$), 611.34 ([**13** − 5Br − 30H$_2$O]$^{5+}$), 496.30 ([**13** − 6Br − 30H$_2$O]$^{6+}$). Anal. Calcd for C$_{76}$H$_{188}$Br$_{12}$Cr$_8$N$_{48}$Ni$_6$O$_{31}$: C, 22.83; H, 4.74; N, 16.82. Found: C, 22.93; H, 4.99; N, 16.61. The solvent content of this compound was confirmed by thermogravimetric analysis.

[(tach)$_8$(H$_2$O)$_6$Cu$_6$Co$_8$(CN)$_{24}$⊃THF]Br$_{12}$·29H$_2$O (14). A solution of **7**·H$_2$O (32 mg, 0.11 mmol) and CuBr$_2$ (81 mg, 0.36 mmol) in 25 mL of water was stirred and concentrated to a volume of 10 mL by heating at reflux. Upon cooling to room temperature, a small amount of gray solid was separated by filtration, and the green filtrate was further concentrated to a volume of 8 mL under reduced pressure. Diffusion of THF vapor into the solution produced blue-green parallelepiped-shaped crystals of **14** suitable for X-ray analysis. The crystals were collected by filtration, washed with successive aliquots of THF (5 mL) and Et$_2$O (5 mL), and dried in air to give 31 mg (53%) of product. IR: ν_{CN} 2198, 2182 (sh) cm^{-1}. μ_{eff} (295 K): 4.67 μ_B. Anal. Calcd for C$_{72}$H$_{198}$Br$_{12}$Co$_8$Cu$_6$N$_{48}$O$_{35}$: C, 21.88; H, 4.78; N, 16.11. Found: C, 21.95; H, 4.93; N, 16.06. The solvent content of this compound was confirmed by thermogravimetric analysis.

[(tach)(H$_2$O)$_3$Co$_2$(CN)$_3$]Br$_2$·5.5H$_2$O (15). A solution of **7**·H$_2$O (0.040 g, 0.14 mmol) and CoBr$_2$ (0.20 g, 0.91 mmol) in 40 mL of water was heated to reflux. Upon concentration to a volume of 2 mL, the solution was cooled to room temperature, and a small amount of unreacted **7**·H$_2$O was removed by filtration. The orange filtrate was further concentrated to a volume of 0.5 mL by evaporation to afford orange platelike crystals suitable for X-ray analysis. The crystals were collected by filtration and dried in air to give 82 mg (91%) of orange product. IR: ν_{CN} 2170 cm^{-1}. Anal. Calcd for C$_9$H$_{32}$Br$_2$Co$_2$N$_6$O$_{8.5}$: C, 16.94; H, 5.06; N, 13.17. Found: C, 17.20; H, 5.22; N, 12.82. The water content of this compound was confirmed by thermogravimetric analysis.

[(tach)(cyclam)NiCr(CN)$_3$](PF$_6$)$_2$·H$_2$O (16). Solid KPF$_6$ (0.12 g, 0.65 mmol) was added to a boiling solution of **17** (0.070 g, 34 μmol) in 15 mL of water. Gradually cooling the solution to room temperature and allowing the volume to reduce to 6 mL prompted formation of yellow-green rectangular plate-shaped crystals of **16**·H$_2$O suitable for X-ray analysis. The crystals were collected by filtration, washed with 2 mL of THF, and dried in air to give 37 mg (66%) of product. Concentrating the filtrate to a volume of 2 mL permitted the recovery of 8 mg of compound **17** in pure form.

IR: ν_{CN} 2158, 2148, 2124, 2117 cm^{-1}. Anal. Calcd for C$_{19}$H$_{41}$CrF$_{12}$N$_{10}$NiOP$_2$: C, 27.62; H, 5.00; N, 16.95. Found: C, 27.70; H, 5.27; N, 16.55. The water content of this compound was confirmed by thermogravimetric analysis.

[(tach)$_2$(cyclam)$_3$Ni$_3$Cr$_2$(CN)$_6$]I$_6$ (17). A solution of **3** (0.10 g, 0.36 mmol) and [Ni(cyclam)I$_2$] (0.28 g, 0.55 mmol) in 125 mL of water was stirred and concentrated to a volume of 50 mL by heating at reflux. The solution was filtered and then gradually cooled to room temperature, prompting formation of 0.21 g of pale green hexagonal plate-shaped crystals suitable for X-ray analysis. Upon further concentrating the solution to a volume of 20 mL via evaporation at room temperature, a second crop of green solid was collected by filtration and dried in air to give a total yield of 0.28 g (75%). IR: ν_{CN} 2144, 2120, 2110 cm^{-1}. μ_{eff} (295 K): 6.22 μ_B. Anal. Calcd for C$_{48}$H$_{102}$Cr$_2$I$_6$N$_{24}$Ni$_3$: C, 28.03; H, 5.00; N, 16.34. Found: C, 28.10; H, 5.18; N, 16.24.

[(tach)$_2$(cyclam)$_3$Cu$_3$Cr$_2$(CN)$_6$](NO$_3$)$_6$ (18). A pink solution of **3** (14 mg, 50 μmol) and [Cu(cyclam)](NO$_3$)$_2$·4H$_2$O (36 mg, 78 μmol) in 20 mL of water was stirred and concentrated to a volume of 10 mL by heating at reflux. The solution was filtered while still hot to remove trace amounts of a gray solid. Concentration of the dark purple filtrate to a volume of 5 mL via evaporation in air afforded yellow crystals of **3** (3 mg), which were removed by filtration. The filtrate was then allowed to stand overnight, resulting in the formation of purple block-shaped crystals suitable for X-ray analysis. The crystals were collected by filtration, washed with 3 mL of THF, and dried in air to give 18 mg (54%) of product. IR: ν_{CN} 2148, 2131 cm^{-1}. Anal. Calcd for C$_{48}$H$_{102}$Cr$_2$Cu$_3$N$_{30}$O$_{18}$: C, 34.27; H, 6.11; N, 24.98. Found: C, 34.62; H, 6.38; N, 25.09.

X-ray Structure Determinations. Structures were determined for the compounds listed in Tables 1−3. Crystals of **8** were found to disintegrate upon cooling in a dinitrogen stream; consequently, a single crystal was coated in epoxy, attached to a glass fiber, transferred to a Siemens SMART diffractometer, and maintained at room temperature. Single crystals of all other compounds were coated with Paratone-N oil, attached to glass fibers, transferred to the diffractometer, and cooled in a dinitrogen stream. Initial lattice parameters were obtained from a least-squares analysis of more than 30 carefully centered reflections; these parameters were later refined against all data. None of the crystals showed significant decay during data collection. Data were integrated and corrected for Lorentz and polarization effects with SAINT and were corrected for absorption effects with SADABS.

Space group assignments were based on systematic absences, E statistics, and successful refinement of the structures. Structures were solved by direct methods with the aid of successive difference Fourier maps and were refined against all data using the SHELXTL

Table 2. Crystallographic Data[a] for **8**, **9**, **10**, **11**, **12·6H₂O**, and **13·11H₂O**

	8	**9**	**10**	**11**	**12·6H₂O**	**13·11H₂O**
formula	$C_{36}H_{120}Br_8$-$Co_4N_{24}Ni_4O_{30}$	$C_{36}H_{100}Br_8$-$Co_8N_{24}O_{20}$	$C_{36}H_{124}Br_8$-$Fe_4N_{23}Ni_4O_{32}$	$C_9H_{47}Br_6Fe$-$N_6Ni_3O_{16}$	$C_{72}H_{192}Br_{12}$-$Cr_8N_{48}Ni_6O_{36}$	$C_{76}H_{210}Br_{12}Cr_8$-$N_{48}Ni_6O_{42}$
formula wt	2479.40	2300.12	2503.11	1206.97	4033.92	4196.10
T, K	295	159	159	142	146	168
space group	$P\bar{4}3m$	$P\bar{4}3m$	$P\bar{4}2m$	$Pnma$	$R\bar{3}$	$C2/c$
Z	1	1	1	4	3	4
a, Å	13.3041(3)	13.403(1)	13.961(5)	11.8248(8)	19.4834(2)	34.1337(8)
b, Å				14.742(1)		19.4024(3)
c, Å			12.822(5)	21.519(1)	37.3386(6)	27.1889(7)
β, deg						114.026(1)
V, Å³	2354.81(9)	2407.8(3)	2499(2)	3751.2(4)	12274.9(3)	16446.5(6)
d_{calc}, g/cm³	1.748	1.586	1.663	2.137	1.637	1.695
R_1 (wR_2),[b] %	8.47 (25.11)	8.71 (23.12)	5.29 (14.04)	5.72 (13.65)	6.93 (18.11)	7.97 (21.77)

[a] Obtained with graphite-monochromated Mo Kα (λ = 0.71073 Å) radiation for **8**, [(tach)₄(H₂O)₁₂Ni₄Co₄(CN)₁₂]Br₈·18H₂O; **9**, [(tach)₄(H₂O)₁₂Co₈-(CN)₁₂]Br₈·8H₂O; **10**, [(tach)₄(H₂O)₁₂Ni₄Fe₄(CN)₁₂]Br₈·20H₂O; **11**, [(tach)(H₂O)₁₅Ni₃Fe(CN)₃]Br₆·H₂O; **12·6H₂O**, [(tach)₈Cr₈Ni₆(CN)₂₄]Br₁₂·36H₂O; and **13·11H₂O**, [(tach)₈Cr₈Ni₆(CN)₂₄⊃THF]Br₁₂·41H₂O. [b] $R_1 = \sum||F_o| - |F_c||/\sum|F_o|$, w$R_2 = \{\sum[w(F_o^2 - F_c^2)^2]/\sum[w(F_o^2)^2]\}^{1/2}$.

Table 3. Crystallographic Data[a] for **14**, **15**, **16·H₂O**, **17**, and **18**

	14	**15**	**16·H₂O**	**17**	**18**
formula	$C_{76}H_{198}Br_{12}Co_8$-$Cu_6N_{48}O_{36}$	$C_9H_{32}Br_2$-$Co_2N_6O_{8.5}$	$C_{19}H_{43}CrF_{12}$-$N_{10}NiO_2P_2$	$C_{48}H_{102}Cr_2$-$I_2N_{24}Ni_3$	$C_{48}H_{102}Cr_2$-$Cu_3N_{30}O_{18}$
formula wt	4172.42	638.09	844.28	1549.47	1682.22
T, K	159	148	155	173	160
space group	$R\bar{3}$	$P2_1/c$	$Pnma$	$R32$	$R\bar{3}$
Z	3	4	4	3	3
a, Å	19.276(1)	14.264(2)	20.832(3)	15.9466(2)	15.8616(2)
b, Å		12.811(2)	16.324(2)		
c, Å	37.008(3)	13.671(2)	9.734(1)	25.4083(5)	25.0846(5)
β, deg		107.173(2)			
V, Å³	11908(2)	2386.7(6)	3310.2(8)	5595.5(2)	5465.5(2)
d_{calc}, g/cm³	1.745	1.776	1.694	1.379	1.533
R_1 (wR_2),[b] %	5.78 (15.06)	4.76 (11.68)	6.46 (18.14)	4.10 (10.27)	3.02 (7.71)

[a] Obtained with graphite-monochromated Mo Kα (λ = 0.71073 Å) radiation for **14**, [(tach)₈(H₂O)₆Cu₆Co₈(CN)₂₄⊃THF]Br₁₂·29H₂O; **15**, [(tach)(H₂O)₃Co₂-(CN)₃]Br₂·5H₂O; **16·H₂O**, [(tach)(cyclam)NiCr(CN)₃](PF₆)₂·2H₂O; **17**, [(tach)₂(cyclam)₃Ni₃Cr₂(CN)₆]I₆; and **18**, [(tach)₂(cyclam)₃Cu₃Cr₂(CN)₆]₂(NO₃)₆. [b] $R_1 = \sum||F_o| - |F_c||/\sum|F_o|$, w$R_2 = \{\sum[w(F_o^2 - F_c^2)^2]/\sum[w(F_o^2)^2]\}^{1/2}$.

5.0 software package. Thermal parameters for all non-hydrogen atoms were refined anisotropically, except for one carbon atom of a tach ligand in **10**, all solvate water molecules in **12·6H₂O** and **13·11H₂O**, and those carbon, nitrogen, or oxygen atoms disordered over multiple partially occupied sites in the structures of **5·2MeOH**, **8·4H₂O**, **8**−**11**, **14**, **15**, **16·H₂O**, and **17**. Hydrogen atoms associated with solvate water or methanol molecules, disordered methylene carbon atoms, and the nitrogen atoms of disordered cyclam ligands were not included in the structural refinements. All other hydrogen atoms were assigned to ideal positions and refined by use of a riding model with an isotropic thermal parameter 1.2 times that of the attached carbon or nitrogen atom (1.5 times for methyl hydrogens). In the structure of **5·2MeOH**, the sodium atom and all of the methanol molecules are disordered over two positions and were modeled accordingly. In the structures of **8·4H₂O**, **10**, and **11** a bromine atom and a water molecule are disordered over two shared positions; the occupancies of these sites were restrained to a sum of one and refined. To balance charge in the structures of **8** and **9**, one bromine atom was restrained to have partial occupancy; in the former case, a water molecule was found to occupy this site the remainder of the time. One nickel and four oxygen atoms in the structure of **11** are disordered by a mirror plane and were modeled accordingly. In the structure of **13·11H₂O**, two nitrogen atoms were subjected to rigid bond restraints, one nitrogen and two carbon atoms were restrained to have the same U_{ij} parameters, and the U_{ij} parameters of the same two carbon atoms were further restrained to approximate isotropic behavior. The THF molecules in the cages of **13·11H₂O** and **14** are disordered over two and six crystallographically distinct orientations, respectively, and were modeled

as such; in the former case, the atoms were refined anisotropically. One nitrogen atom and four methylene carbon atoms of the cyclam ligand in the structure of **17** were modeled as being disordered over two equally occupied sites, corresponding to two distinct cyclam ligand conformations. Five of the solvate water molecules in the structure of **8** were modeled as being disordered over several positions. Three of the solvate water molecules in each of the structures of **8**, **9**, and **15** were treated similarly, as were four of the solvate water molecules in **10**, six of the bromine atoms in **12·6H₂O**, 14 of the solvate water molecules in **13·11H₂O**, two of the bromine atoms and five of the solvate water molecules in **14**, and four of the fluorine atoms in **16·H₂O**. The final agreement factors (Tables 1−3) for the structures of **5·2MeOH**, **8**, **9**, and **13·11H₂O** are high owing to the extensive disorder present in the crystals and the accompanying poor quality of the data.

Magnetic Susceptibility Measurements. DC magnetic susceptibility data were collected on a Quantum Design MPMS2 SQUID magnetometer at temperatures ranging from 5 to 295 K. Data were corrected for diamagnetic contributions by use of Pascal's constants. A temperature-independent paramagnetism of 200×10^{-6} cgsu per metal center (Fe^III excluded) was assumed for each compound. Samples for magnetization measurements were suspended in eicosane to prevent torquing of the crystallites at high magnetic fields. For the purpose of modeling the exchange interactions, the orbital contributions of the low-spin Fe^III ions in compounds **10** and **11** were eliminated from the data by a previously published procedure.[19] Theoretical models were fit to susceptibility data for compound **11** with a relative error minimization routine (MAGFIT

3.1).[20] For compound **10**, data were simulated by use of MAG-PACK.[21] Reported coupling constants are based on exchange Hamiltonians of the form $\hat{H} = -2J\hat{S}_i\cdot\hat{S}_j$.

Other Physical Measurements. Absorption spectra were measured with a Hewlett-Packard 8453 spectrophotometer. Infrared spectra were recorded on a Nicolet Avatar 360 FTIR spectrometer equipped with an attenuated total reflectance accessory. Mössbauer spectra were collected with a constant-acceleration spectrometer that employed a rhodium matrix cobalt-57 source and was calibrated at room temperature with α-iron foil. Mass spectrometric measurements were performed in the positive ion mode on a VG Quattro (Micromass) spectrometer or on a Bruker Apex II 7 T actively shielded FT-ICR mass spectrometer, both of which were equipped with an analytical electrospray ion source instrument. Thermogravimetric analyses were carried out in a dinitrogen atmosphere with a TA Instruments TGA 2950. Electrochemical measurements were conducted with a Bioanalytical Systems CV-50 potentiostat with platinum disk working, platinum wire auxiliary, and silver wire reference electrodes. Samples were measured with 0.1 M $(Bu_4N)BF_4$ as the supporting electrolyte, and ferrocene was added as an internal reference after each measurement.

Results and Discussion

Tricyanide Complexes. Convenient preparations of the complexes [(tach)M(CN)$_3$] (M = Cr, Fe, Co) largely parallel those of the analogous tacn-ligated compounds. Several attempts to substitute cyanide for triflate in the previously reported [(tach)Cr(CF$_3$SO$_3$)$_3$] complex[22] failed to afford a clean product. Consequently, a less direct route, emulating the synthesis of [(tacn)Cr(CN)$_3$],[23] was developed. The reaction of Cr(CO)$_6$ with tach in mesitylene provides [(tach)-Cr(CO)$_3$] (**1**), which is readily oxidized with bromine to yield [(tach)CrBr$_3$] (**2**). This hygroscopic blue-green compound is insoluble in most common solvents but dissolves in DMSO to give a purple solution. Subsequent addition of an excess of NaCN generates the tricyanide complex, [(tach)Cr(CN)$_3$]· H$_2$O (**3**). The magnetic moment of 3.89 μ_B measured for compound **3** at room temperature is consistent with the expected $S = \frac{3}{2}$ ground state.

The synthesis of [(tach)Fe(CN)$_3$] proceeds via the intermediate iron(II) complexes [(tach)Fe(CF$_3$SO$_3$)$_2$(MeCN)] and [(tach)Fe(CN)$_3$]$^{1-}$. The reaction of Fe(CF$_3$SO$_3$)$_2$ with tach in acetonitrile gives a purple solution, from which tan-colored [(tach)Fe(CF$_3$SO$_3$)$_2$]·0.4MeCN (**4**) precipitates upon addition of ether. The dependence of the color on the amount of associated acetonitrile is similar to the behavior reported for the analogous Me$_3$tacn-containing complex.[15] Compound **4** is soluble in a variety of polar solvents, including methanol, acetonitrile, and DMF, and rapidly oxidizes in air. X-ray analysis of crystals of **4**·0.6MeCN grown by diffusion of

ether into an acetonitrile solution revealed a central iron atom octahedrally coordinated by the tach ligand, an acetonitrile molecule, and an oxygen atom from each of the two triflate anions (see Figure S1 in the Supporting Information). Reaction of **4** with a slight excess[24] of NaCN in DMF induces formation of an orange precipitate, which can be recrystallized from methanol as Na[(tach)Fe(CN)$_3$]·MeOH (**5**). On the basis of its variation with temperature (see Figure S2 in the Supporting Information), the substantial effective magnetic moment of 1.30 μ_B observed for **5** at room temperature is attributed to temperature-independent paramagnetism. Mössbauer spectra collected at 295 and 90 K confirm the assignment of the metal center as low-spin iron(II), and exclude the possibility of spin equilibrium behavior.

Chemical oxidation of [(tach)Fe(CN)$_3$]$^{1-}$ readily supplies the intended [(tach)Fe(CN)$_3$] complex. The cyclic voltammogram of compound **5** in methanol features an oxidation process corresponding to the [(tach)Fe(CN)$_3$]$^{1-/0}$ couple centered at $E_{1/2} = -0.470$ V ($\Delta E_p = 122$ mV) versus the Cp$_2$Fe$^{0/1+}$ couple. For comparison, the analogous [(Me$_3$tacn)-Fe(CN)$_3$]$^{1-/0}$ couple in methanol occurs at the slightly higher potential of $E_{1/2} = -0.297$ V.[25] Treatment of **5** with iodine in methanol produces a yellow precipitate, which, upon washing with water, analyzes as [(tach)Fe(CN)$_3$]·H$_2$O (**6**). The effective magnetic moment of **6** at room temperature is 2.63 μ_B, considerably higher than the spin-only moment of 1.73 μ_B expected for an $S = \frac{1}{2}$ ground state with $g = 2.00$. As the temperature is lowered, the moment decreases, attaining a value of 1.99 μ_B at 5 K (see Figure S3 in the Supporting Information). This behavior is typical for octahedral complexes of low-spin iron(III), originating from unquenched orbital angular momentum.[26] Indeed, Mössbauer spectra collected at 295 and 90 K are consistent with assignment of the complex as low-spin and again exclude the possibility of spin equilibrium behavior. The X-band EPR spectrum of **6**, measured at 14 K as a 5% (w/w) solid solution in diamagnetic [(tach)Co(CN)$_3$]·H$_2$O, exhibits an axial signal with $g_\perp = 1.55$ and $g_\parallel = 3.35$ (see Figure S4 in the Supporting Information). Such a highly anisotropic **g** tensor is not uncommon among low-spin iron(III) complexes,[27] and these values are particularly reminiscent of certain substituted ferricenium salts.[28]

As previously reported,[18a] the synthesis of [(tach)Co-(CN)$_3$]·H$_2$O (**7**·H$_2$O) proceeds through a direct synthesis of [(tach)CoCl$_3$], followed by reaction with KCN. Unfortunately, this approach seems not to extend to other transition metal ions.

The crystal structures of [(tach)Cr(CN)$_3$]·H$_2$O (**3**), Na-[(tach)Fe(CN)$_3$]·3MeOH (**5**·2MeOH), [(tach)Fe(CN)$_3$]·H$_2$O

(19) (a) Colacio, E.; Ghazi, M.; Stoeckli-Evans, H.; Lloret, F.; Moreno, J.-M.; Pérez, C. *Inorg. Chem.* **2001**, *40*, 4876. (b) Lescouëzec, R.; Lloret, F.; Julve, M.; Vaissermann, J.; Verdaguer, M. *Inorg. Chem.* **2002**, *41*, 818.
(20) Schmitt, E. A. Ph.D. Thesis, University of Illinois at Urbana−Champaign, 1995.
(21) Borrás-Almenar, J. J.; Clemente-Juan, J. M.; Coronado, E.; Tsukerblat, B. S. *J. Comput. Chem.* **2001**, *22*, 985.
(22) Glerup, J.; Weihe, H.; Goodson, P. A.; Hodgson, D. J. *Inorg. Chim. Acta* **1993**, *212*, 281.
(23) Kirk, A. D.; Namasivayam, C. *Inorg. Chem.* **1988**, *27*, 1095.

(24) Use of a large excess of NaCN results in the formation of significant amounts of Na$_4$[Fe(CN)$_6$], as determined by infrared spectroscopy.
(25) Moreland, A. C.; Rauchfuss, T. B. *Inorg. Chem.* **2000**, *39*, 3029.
(26) Figgis, B. N.; Lewis, J.; Mabbs, F. E.; Webb, G. A. *J. Chem. Soc. A* **1966**, 422.
(27) (a) Rieger, P. H. *Coord. Chem. Rev.* **1994**, *135/136*, 203. (b) Bencini, A.; Gatteschi, D. In *Transition Metal Chemistry: A Series of Advances*. Melson, G. A., Figgis, B. N., Eds.; Marcel Dekker: New York, 1982; Vol. 8.
(28) (a) Prins, R.; Korswagen, A. R. *J. Organomet. Chem.* **1970**, *25*, C74. (b) Duggan, D. M.; Hendrickson, D. N. *Inorg. Chem.* **1975**, *14*, 955.
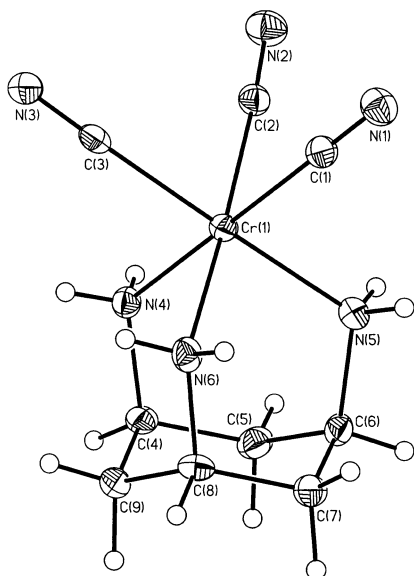
Figure 1. Structure of the [(tach)Cr(CN)$_3$] complex in **3**, showing 40% probability ellipsoids.

Table 4. Selected Mean Interatomic Distances and Angles[a] for the [(tach)M(CN)$_3$]$^{0,1-}$ Complexes in the Structures of **3**, **5·2MeOH**, **6**, and **7**

	M = Cr^{III}	M = Fe^{II}	M = Fe^{III}	M = Co^{III}
M−C	2.081(8)	1.90(1)	1.931(5)	1.888(6)
M−N	2.078(9)	2.06(1)	2.017(6)	1.997(1)
C−N$_{CN}$[b]	1.15(1)	1.16(1)	1.159(6)	1.154(1)
C−N$_{tach}$[b]	1.494(5)	1.48(3)	1.494(1)	1.487(5)
M−C−N	177.5(6)	176.9(2)	178.1(8)	177(3)
M−N−C	118.0(1)	119.0(3)	118.4(1)	118.1(5)
C−M−C	87.8(3)	91(2)	87(1)	90(2)
C−M−N	92(1)	90(1)	92(1)	90.3(6)
N−M−N	89(1)	88.3(2)	90(1)	90.1(9)

[a] Distances are given in angstroms; angles are given in degrees. [b] N$_{CN}$ and N$_{tach}$ indicate N atoms in cyanide and tach ligands, respectively.

(**6**), and [(tach)Co(CN)$_3$] (**7**) were determined by single-crystal X-ray analysis. Each tricyanide complex displays the *fac* stereochemistry expected for octahedral coordination by a tridentate tach ligand and three terminal cyanide ligands; Figure 1 depicts the structure of the [(tach)Cr(CN)$_3$] complex as a representative example. Selected mean interatomic distances and angles for all four complexes are compared in Table 4. Overall, the bond distances and angles are similar, the main exception being the mean M−C distance, which decreases along the sequence M = Cr^{III}, Fe^{III}, Fe^{II}, Co^{III}. The trend nicely parallels that observed for the analogous hexacyanometalates, which, as potassium salts, display mean M−C distances of 2.08(2), 1.938(8), 1.92(5), and 1.89(2) Å, respectively.[29] Note that, as judged by the N−M−N angles, the coordination of the metal centers in these tach complexes more closely approaches an ideal octahedral geometry than in the analogous tacn complexes.

Cubic M′$_4$M$_4$(CN)$_{12}$ Clusters. When tacn is employed as a capping ligand, reactions targeting a cubic M′$_4$M$_4$(CN)$_{12}$

(29) (a) Pospelov, V. A.; Zhdanov, G. S. *Zh. Fiz. Khim.* **1947**, *21*, 879. (b) Jagner, S.; Ljungström, E.; Vannerberg, N.-G. *Acta Chem. Scand.* **1974**, *A28*, 623. (c) Figgis, B. N.; Skelton, B. W.; White, A. H. *Aust. J. Chem.* **1978**, *31*, 1195. (d) Reynhardt, E. C.; Boeyens, J. C. A. *Acta Crystallogr.* **1972**, *B28*, 524.
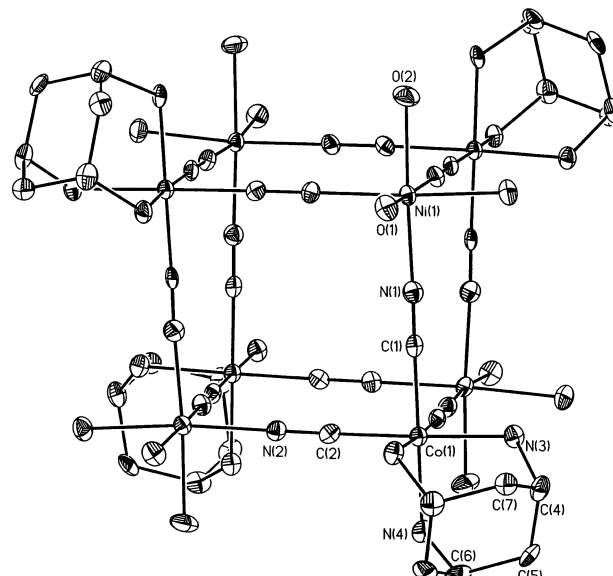
Figure 2. Structure of the cubic [(tach)$_4$(H$_2$O)$_{12}$Ni$_4$Co$_4$(CN)$_{12}$]$^{8+}$ cluster in **8·4H$_2$O**, showing 40% probability ellipsoids; H atoms are omitted for clarity. The cluster resides on a $\bar{4}2m$ symmetry site in the crystal, with the Ni(1)−O(2) bonds running approximately parallel to the $\bar{4}$ axis.

cluster appear to require its presence on both precursor complexes, as exemplified by reaction 1 above.[9a] Unexpectedly, it was discovered that this requirement does not hold when tach is used as a capping ligand. Rather, the hydrogen-bonding capabilities of tach enable stabilization of a cubic cluster with just water as a terminal ligand on the second type of metal center:

$$4[(\text{tach})M(CN)_3] + 4[M'(H_2O)_6]^{2+} \rightarrow$$
$$[(\text{tach})_4(H_2O)_{12}M'_4M_4(CN)_{12}]^{8+} \quad (3)$$
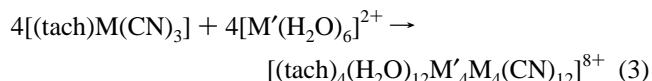
In accord with this reaction, concentration of aqueous solutions containing [(tach)M(CN)$_3$] (M = Fe or Co) and an excess of M′Br$_2$ (M′ = Co or Ni) produces, upon drying in air, [(tach)$_4$(H$_2$O)$_{12}$Ni$_4$Co$_4$(CN)$_{12}$]Br$_8$·23H$_2$O (**8·5H$_2$O**), [(tach)$_4$(H$_2$O)$_{12}$Co$_8$(CN)$_{12}$]Br$_8$·8H$_2$O (**9**), and [(tach)$_4$(H$_2$O)$_{12}$-Ni$_4$Fe$_4$(CN)$_{12}$]Br$_8$·18H$_2$O (**10**). These compounds are quite hygroscopic, such that the water content can vary considerably with humidity and drying conditions. Furthermore, they dissolve only in water, where, on the basis of infrared spectra, they dissociate back into the [(tach)M(CN)$_3$] and [M′-(H$_2$O)$_6$]$^{2+}$ precursor complexes.

X-ray analyses of single crystals of **8·4H$_2$O**, **8**, **9**, and **10**, revealed structures containing [(tach)$_4$(H$_2$O)$_{12}$M′$_4$M$_4$(CN)$_{12}$]$^{8+}$ clusters, all with a common cubic geometry. As a representative example, Figure 2 depicts the structure of the [(tach)$_4$-(H$_2$O)$_{12}$Ni$_4$Co$_4$(CN)$_{12}$]$^{8+}$ cluster in **8**. Its core is analogous to that previously observed for [(tacn)$_8$Co$_8$(CN)$_{12}$]$^{12+}$,[9a,b] consisting of Co^{III} and Ni^{II} ions arranged at alternating vertexes of a cube and connected through cyanide bridges that span each cube edge. This motif represents the fundamental cage unit in the Prussian blue structure type,[13] isolated by virtue of the outer capping ligands: tach on the Co^{III} centers and three water molecules on each Ni^{II} center. Note that the Co^{III}-C-N-Ni^{II} connectivity of the cluster maintains

Table 5. Selected Mean Interatomic Distances and Angles for the Cubic Clusters in the Structures of **8·4H₂O**, **8**, **9**, and **10**[a]

	8·4H₂O	**8**	**9**	**10**
M–C	1.896(4)	1.89(2)	1.88(3)	1.937(9)
M–N	1.991(7)	1.96(2)	2.03(2)	2.016(9)
M′–N	2.028(8)	2.01(2)	2.09(3)	2.02(2)
M′–O	2.10(3)	2.18(2)	2.07(2)	2.10(3)
C–N$_{CN}$	1.14(2)	1.16(2)	1.15(3)	1.15(1)
M···M′	5.062(4)	5.051	5.115	5.111(1)
M–C–N	178.4(4)	174(2)	173(2)	176.7(6)
M′–N–C	178(2)	176(2)	176(2)	177(3)
C–M–C	88(1)	88.5(8)	91(1)	87(2)
C–M–N	90.6(6)	88.8(6)	89.9(7)	90.8(4)
N–M–N	91(1)	93.7(9)	88.8(8)	91(2)
N–M′–N	95(2)	92.8(9)	93.6(7)	95(1)
N–M′–O	90(1)	92.0(7)	89.2(6)	89.8(7)
O–M′–O	86.2(2)	82.8(8)	88(1)	86.0(3)

[a] M = Co, Fe; M′ = Ni, Co; N$_{CN}$ indicates an N atom in a cyanide ligand. Distances are given in angstroms and angles are given in degrees for **8·4H₂O**, [(tach)₄(H₂O)₁₂Ni₄Co₄(CN)₁₂]Br₈·22H₂O; **8**, [(tach)₄(H₂O)₁₂Ni₄Co₄(CN)₁₂]Br₈·18H₂O; **9**, [(tach)₄(H₂O)₁₂Co₈(CN)₁₂]Br₈·8H₂O; and **10**, [(tach)₄(H₂O)₁₂Ni₄Fe₄(CN)₁₂]Br₈·20H₂O.

the cyanide ligand orientation of the [(tach)Co(CN)₃] precursor complex. Indeed, consistent with the site preferences established for Prussian blue-type solids,[30] no evidence for cyanide linkage isomerization is apparent in either the structures or physical properties of compounds **8–10**. Selected mean interatomic distances and angles from all four crystal structures are provided in Table 5 for comparison. As reflected primarily in the N–M′–N angles of greater than 90°, each cluster deviates slightly from a perfect cube. Interestingly, the cyanide bridges in the structures of **8** and **9**, occurring in cubic space group $P\bar{4}3m$, are somewhat more bent than those in the structures of **8·4H₂O** and **10**, occurring in tetragonal space group $P\bar{4}2m$. The major difference between these two structure types lies in the hydrogen-bonded network immediately surrounding the clusters. As depicted for **8·4H₂O** and **8** in Figure 3, one structure contains clusters surrounded by eight bromide anions and 40 water molecules, while the clusters in the other structure are surrounded by 48 bromide anions. Each surrounding entity is involved in hydrogen bonding with both a tach ligand and a water ligand of the cluster, such that two N–H···Br··· H–O or N–H···O–H···O (or perhaps N–H···O···H–O) interactions support every edge of the cube. Presumably, it is these interactions that are responsible for stabilizing the cubic cluster geometry despite the presence of tach ligands on only half of the vertexes.

The metal–cyanide cage of each [(tach)₄(H₂O)₁₂M′₄M₄-(CN)₁₂]⁸⁺ cluster defines a central cavity with a minimum diameter of 3.9 Å, based on van der Waals radii.[31] Access to the cavity is readily available through the square openings of the cube faces, which have a minimum diameter of 1.8 Å.[31] Significantly, as crystallized from aqueous solution, none of the structures features a water molecule within the confines of the cluster cage. Similar behavior has been described

(30) Shriver, D. F.; Shriver, S. A.; Anderson, S. E. *Inorg. Chem.* **1965**, *4*, 725.

(31) van der Waals radii of 1.20, 1.71, 1.55, and 1.91 Å were assumed for H, C, N, and Ni atoms, respectively: Batsanov, S. S. *Russ. Chem. Bull.* **1995**, *44*, 18.
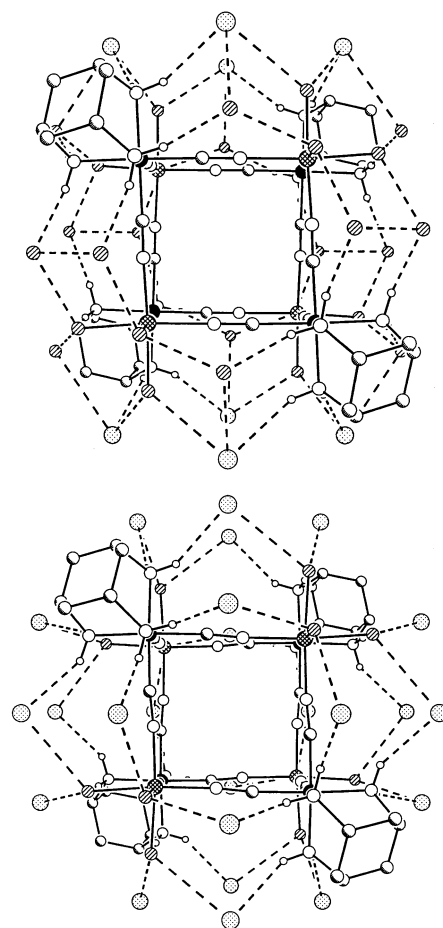
Figure 3. Hydrogen-bonding interactions surrounding the [(tach)₄(H₂O)₁₂-Ni₄Co₄(CN)₁₂]⁸⁺ clusters in the structures of **8·4H₂O** (upper panel) and **8** (lower panel). Black, crosshatched, shaded, larger white, smaller white, hatched, and dotted spheres represent Co, Ni, C, N, H, O, and Br atoms, respectively; only H atoms bound to N atoms are shown. In the upper structure, the cluster resides on a $\bar{4}2m$ symmetry site (with the $\bar{4}$ axis running along the vertical direction), while in the lower structure, the cluster resides on a $\bar{4}3m$ symmetry site.

previously for the [(tacn)₈Co₈(CN)₁₂]¹²⁺ cluster.[9a,b] The absence of a guest water molecule in these species is assumed to be a consequence of the hydrophobic nature of the cavity and the availability of facile escape routes upon or during cage formation. Indeed, while it is clear that alkali metal cations can occupy such positions, we could find no detailed structural analysis confirming the presence of water within the analogous cages of a Prussian blue-type solid possessing a fully occupied metal–cyanide lattice.

Compounds **8** and **9** contain clusters in which paramagnetic metal centers are directly linked through cyanide only to metal centers that are diamagnetic. Accordingly, the value of $\chi_M T = 5.55$ cm³·K/mol observed for **8** at room temperature is consistent with four noninteracting Ni^{II} ions, each with a spin of $S = 1$ and $g = 2.36$.

In contrast, the metal centers in the [(tach)₄(H₂O)₁₂Ni₄-Fe₄(CN)₁₂]⁸⁺ cluster of **10** are all paramagnetic—alternating between Fe^{III} ($S = ¹/_2$) and Ni^{II} ($S = 1$)—and engage in magnetic exchange coupling. The variation of $\chi_M T$ with temperature for this compound is plotted as the squares in the upper panel of Figure 4. At 295 K, $\chi_M T$ is 8.48 cm³·K/mol, somewhat above the spin-only value of 5.50 cm³·K/

mol expected for four $S = \frac{1}{2}$ and four $S = 1$ ions in the absence of exchange coupling. The difference is largely accounted for by assuming that *g* is greater than 2.00, in line with the observed moments of compounds **6** and **8**. However, as the temperature is lowered, $\chi_M T$ increases monotonically, attaining a value of 23.44 cm³·K/mol at 6 K. This behavior is consistent with an $S = 6$ ground state stemming from ferromagnetic exchange coupling, as predicted[11] to arise between octahedrally coordinated Fe^{III} (t_{2g}^5) and Ni^{II} ($t_{2g}^6 e_g^2$) centers bridged by cyanide. Determining the strength of this exchange interaction is complicated by the presence of unquenched orbital angular momentum on the Fe^{III} sites in the cluster. The orbital contribution for each Fe^{III} center was therefore eliminated from the data by subtracting the values of $\chi_M T$ observed for [(tach)Fe(CN)$_3$] in **6** and replacing them with a constant value of 0.375 cm³·K/mol (corresponding to a spin-only ion with $S = \frac{1}{2}$ and $g = 2.00$). The corrected data—shown as the circles in the upper panel of Figure 4—were simulated by use of MAGPACK and an exchange Hamiltonian of the form

$$\hat{H} = -2J[\hat{S}_{Ni(1)} \cdot (\hat{S}_{Fe(1)} + \hat{S}_{Fe(2)} + \hat{S}_{Fe(3)}) + \hat{S}_{Ni(2)} \cdot (\hat{S}_{Fe(1)} + \hat{S}_{Fe(2)} + \hat{S}_{Fe(4)}) + \hat{S}_{Ni(3)} \cdot (\hat{S}_{Fe(1)} + \hat{S}_{Fe(3)} + \hat{S}_{Fe(4)}) + \hat{S}_{Ni(4)} \cdot (\hat{S}_{Fe(2)} + \hat{S}_{Fe(3)} + \hat{S}_{Fe(4)})] \quad (4)$$

The best match was obtained with $J = 5.5$ cm^{-1} and $g = 2.16$, indicating that the exchange coupling within the [(tach)$_4$(H$_2$O)$_{12}$Ni$_4$Fe$_4$(CN)$_{12}$]$^{8+}$ cluster is ferromagnetic but rather weak. This is in agreement with the behavior observed for other cyanide-bridged molecules containing low-spin iron(III) and high-spin nickel(II): fits to the susceptibility data for the trigonal bipyramidal clusters {[Ni(bpm)$_2$]$_3$[Fe(CN)$_6$]$_2$} [where bpm = bis(1-pyrazol)methane] and {[Ni(IM-2Py)$_2$]$_3$[Fe(CN)$_6$]$_2$} [where IM-2Py = (2-pyridyl)-substituted imino nitroxide] gave *J* values of 5.3 and 3.4 cm^{-1}, respectively.[33] A slightly stronger coupling of $J = 9.4$ cm^{-1} has been estimated for the Prussian blue analogue Ni$_3$[Fe(CN)$_6$]$_2 \cdot x$H$_2$O.[34]

A Trigonal Pyramidal Ni$_3$Fe(CN)$_3$ Cluster. Owing in part to the low solubility of [(tach)Fe(CN)$_3$] in water, an excess of [Ni(H$_2$O)$_6$]$^{2+}$ is required for generating cube-containing **10** in reasonable quantities. As the relative concentration of [(tach)Fe(CN)$_3$] in the reaction solution drops, however, a new nickel-rich compound, [(tach)(H$_2$O)$_{15}$-Ni$_3$Fe(CN)$_3$]Br$_6 \cdot$H$_2$O (**11**), begins to emerge. Once precipitation of **10** has ceased, **11** can be isolated in pure form as green rod-shaped crystals. A similar procedure was found to yield the cobalt-containing analogue [(tach)(H$_2$O)$_{15}$Ni$_3$-Co(CN)$_3$]Br$_6 \cdot$H$_2$O.

X-ray analysis of a single crystal of **11** showed the compound to contain the trigonal pyramidal [(tach)(H$_2$O)$_{15}$-
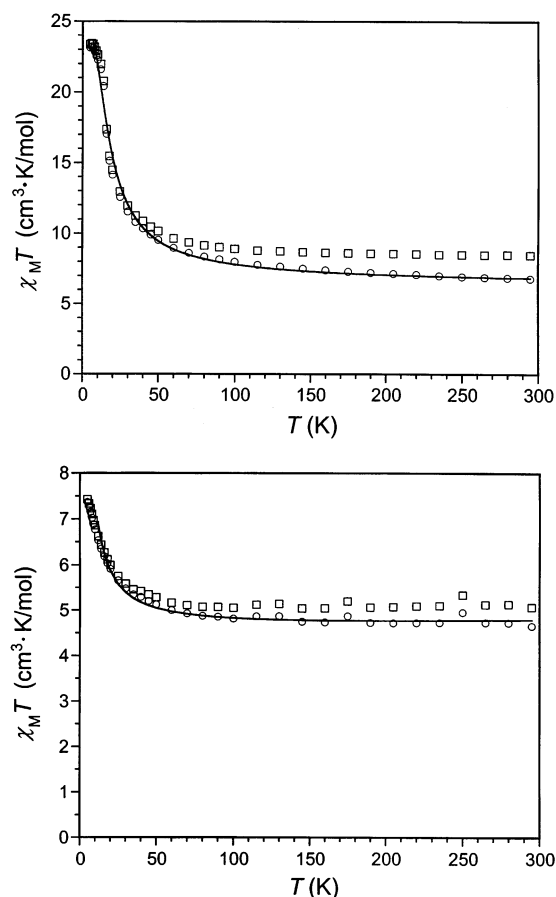
Figure 4. Magnetic behavior of [(tach)$_4$(H$_2$O)$_{12}$Ni$_4$Fe$_4$(CN)$_{12}$]Br$_8 \cdot$20H$_2$O (**10**, upper panel) and [(tach)(H$_2$O)$_{15}$Ni$_3$Fe(CN)$_3$]Br$_6 \cdot$2H$_2$O (**11**·H$_2$O, lower panel), as measured in an applied field of 1000 G. Squares and circles represent data before and after subtracting the orbital contribution of the [(tach)Fe(CN)$_3$] component(s), respectively. The solid lines represent calculated fits to the adjusted data.

Ni$_3$Fe(CN)$_3$]$^{6+}$ cluster depicted in Figure 5. The cluster consists of a central [(tach)Fe(CN)$_3$] moiety with a [Ni(H$_2$O)$_5$]$^{5+}$ unit appended at the nitrogen end of each cyanide ligand. Other than having slightly more bent Ni–N–C angles, its interatomic distances and angles (see Figure 5 caption) do not much deviate from those in the structure of **10** (see Table 5). Indeed, with a maximal point group symmetry of C_{3v}, the cluster closely approximates a fragment of the [(tach)$_4$(H$_2$O)$_{12}$Ni$_4$Fe$_4$(CN)$_{12}$]$^{8+}$ cube. Cyano-bridged species possessing a related trigonal pyramidal core geometry have been previously realized in the forms of {(THF)$_3$Cr-[NCCr(CO)$_5$]$_3$} and [(edma)$_3$Cu$_3$Cr(CN)$_6$] (where edma = ethylenediaminemonoacetate).[35] Unlike in **10**, the clusters in crystals of **11** are directly linked to one another through hydrogen bonds. One amino group of the tach ligand interacts with two water ligands from a neighboring cluster, each at an N···O separation of 3.465(9) Å, to form a one-dimensional chain that propagates through the structure (see Figure S5 in the Supporting Information).

The magnetic behavior of **11**·H$_2$O again indicates weak ferromagnetic coupling between the Fe^{III} and Ni^{II} centers.

(32) This footnote was deleted on revision.
(33) (a) Langenberg, K. V.; Batten, S. R.; Berry, K. J.; Hockless, D. C. R.; Moubaraki, B.; Murray, K. S. *Inorg. Chem.* **1997**, *36*, 5006. (b) Vostrikova, K. E.; Luneau, D.; Wernsdorfer, W.; Rey, P.; Verdaguer, M. *J. Am. Chem. Soc.* **2000**, *122*, 718.
(34) Juszczyk, S.; Johansson, C.; Hanson, M.; Ratuszna, A.; Malecki, G. *J. Phys.: Condens. Matter* **1994**, *6*, 5697.

(35) (a) Edelmann, F.; Behrens, U. *J. Organomet. Chem.* **1977**, *131*, 65. (b) Fu, D. G.; Chen, J.; Tan, X. S.; Jiang, L. J.; Zhang, S. W.; Zheng, P. J.; Tang, W. X. *Inorg. Chem.* **1997**, *36*, 220.
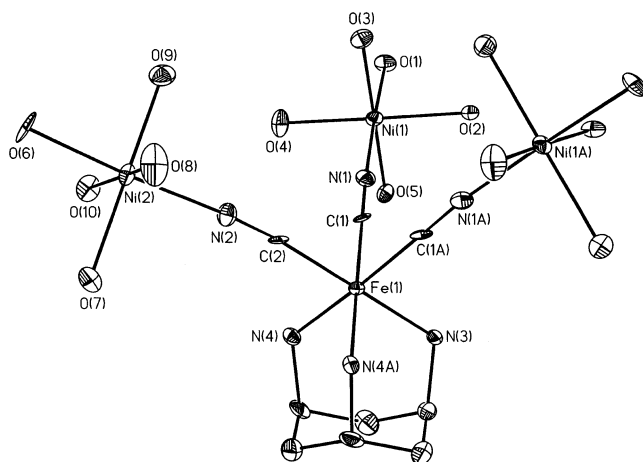
Figure 5. Structure of the $[(tach)(H_2O)_{15}Ni_3Fe(CN)_3]^{6+}$ cluster in **11**, showing 40% probability ellipsoids; H atoms are omitted for clarity. The molecule resides on a crystallographic mirror plane that interrelates atoms Ni(1) and Ni(1A). The atoms Ni(2), O(5), O(6), O(8), and O(9) are disordered about the mirror plane; only one orientation is shown here. Selected mean interatomic distances (angstroms) and angles (degrees): Fe−C 1.933(2), Fe−N 2.017(8), Ni−N 2.009(7), Ni−O 2.07(2), C−N$_{CN}$ 1.155(7), Fe···Ni 5.079(9), Fe−C−N 177(3), Ni−N−C 172(5), C−Fe−C 88(1), C−Fe−N 90.9(9), N−Fe−N 91(1), N−Ni−O 90(2), O−Ni−O 90-(2).

The lower panel of Figure 4 shows the variation of $\chi_M T$ with temperature for this compound, which is quite analogous to that observed for **10** (upper panel). The steady rise of $\chi_M T$ with decreasing temperature likewise signifies the expected[11] ferromagnetic exchange interactions, in this instance leading to an $S = {}^7/_2$ ground state. To estimate the strength of the magnetic coupling, the orbital contribution of the Fe^{III} center was eliminated from the susceptibility data by a procedure identical to that described above for analyzing the data from compound **10**. The resulting data are plotted as circles in Figure 4 and were fit with MAGFIT 3.1 and an exchange Hamiltonian of the form

$$\hat{H} = -2J[\hat{S}_{Fe} \cdot (\hat{S}_{Ni(1)} + \hat{S}_{Ni(2)} + \hat{S}_{Ni(3)})] \qquad (5)$$

The best fit gave $J = 1.2$ cm^{-1} and $g = 2.29$, suggesting that the coupling is significantly weaker than in **10**. This discrepancy could potentially arise from attenuation of the ferromagnetic coupling in **11**·H_2O by weak antiferromagnetic coupling mediated through the aforementioned Fe−N−H···O−Ni interactions between neighboring clusters. Such hydrogen-bonded pathways have been invoked previously in rationalizing the origin of magnetic coupling in numerous related situations.[9e,33a,36]

Face-Centered Cubic Cr$_8$Ni$_6$(CN)$_{24}$ and Cu$_6$Co$_8$(CN)$_{24}$ Clusters. Paralleling the role of $[(Me_3tacn)Cr(CN)_3]$ in reaction 2 above,[9b] $[(tach)Cr(CN)_3]$ reacts with $[Ni(H_2O)_6]^{2+}$ in aqueous solution to afford the anticipated $[(tach)_8Cr_8Ni_6-(CN)_{24}]^{12+}$ cluster. Subsequent addition of acetonitrile induces precipitation of the bromide salt as $[(tach)_8Cr_8Ni_6(CN)_{24}]Br_{12}$·$30H_2O$ (**12**). The compound is soluble only in water, and infrared spectroscopy and electrospray mass spectrometry experiments indicate that the cluster remains intact in solution.

(36) Desplanches, C.; Ruiz, E.; Rodríguez-Fortea, A.; Alvarez, S. *J. Am. Chem. Soc.* **2002**, *124*, 5197 and references therein.
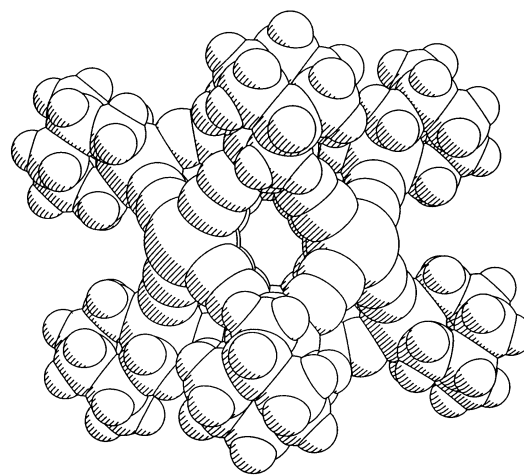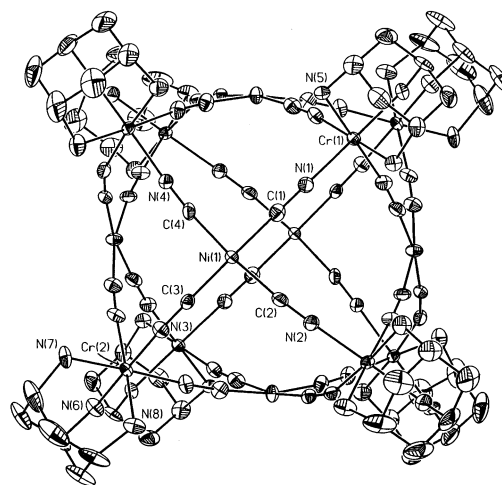
Figure 6. Structure of the face-centered cubic $[(tach)_8Cr_8Ni_6(CN)_{24}]^{12+}$ cluster in **12**·6H_2O. Upper panel: ORTEP diagram showing 50% probability ellipsoids; H atoms are omitted for clarity. The cluster resides on a $\bar{3}$ symmetry site in the crystal, with the 3-fold rotation axis penetrating the Cr(1) atom. Lower panel: Space-filling model, as viewed down an opening along a cube edge.

X-ray analysis of a single crystal of **12**·6H_2O revealed the $[(tach)_8Cr_8Ni_6(CN)_{24}]^{12+}$ cluster to comprise a slightly distorted version of the usual face-centered cubic geometry.[9b,e] Its structure, shown at the top of Figure 6, consists of an approximate cube of eight tach-capped Cr^{III} ions, with all six faces spanned by square planar $[Ni(CN)_4]^{2-}$ units. Thus, as observed previously for $[(Me_3tacn)_8Cr_8Ni_6(CN)_{24}]^{12+}$,[9b] formation of the cluster entails a cyanide linkage isomerization process in which the original Cr^{III}−C−N−Ni^{II} bridging arrangement is transformed into the thermodynamically favored[30] Cr^{III}−N−C−Ni^{II} arrangement. [Accordingly, the Ni^{II} centers are diamagnetic, and compound **12** exhibits an effective magnetic moment at room temperature that is consistent with eight isolated Cr^{III} ($S = {}^3/_2$) centers.] Selected interatomic distances and angles from the structure are listed in Table 6, along with those of $[(Me_3tacn)_8Cr_8Ni_6(CN)_{24}]^{12+}$ for comparison. The main differences in the core geometries of the two clusters stem from a distortion of the tach-ligated species away from the ideal O_h symmetry. This distortion takes the form of a trigonal compression along a body diagonal of the Cr$_8$ cube that coincides with a 3-fold rotation axis (the c axis) of the crystal. The compression is particularly

Table 6. Selected Mean Interatomic Distances and Angles for the Face-Centered Cubic Clusters in the Structures of Me₃tacn, **12·6H₂O**, **13·11H₂O**, and **14**[a]

	Me₃tacn	**12·6H₂O**	**13·11H₂O**	**14**
M−X	2.031(7)	2.01(1)	2.02(1)	1.880(9)
M′−X	1.873(9)	1.851(7)	1.86(1)	1.96(1)
X−X	1.145(6)	1.15(2)	1.15(2)	1.15(1)
M−N$_{tac}$	2.066(5)	2.036(4)	2.05(1)	1.982(8)
Cu−O				2.265(7)
M···M′	5.019(2)	4.98(4)	4.98(4)	4.94(4)
M···M	6.97(2)	6.584	6.61(3)	6.7(2)
		7.160	7.15(7)	7.085
trans-M′···M′	8.844	8.994	9.0(2)	9.100
X−M−X	88.0(3)	90(2)	90(2)	88(2)
M−X−X	169.1(5)	157.1(8)	158(2)	177(3)
		176(1)	174(2)	
X−M′−X	89.6(3)	90(3)	90(3)	89(2)
	170.0(5)	169(2)	170(1)	167(4)
M′−X−X	177(2)	174(2)	173(2)	158.4
				171(3)
X−M−N$_{tac}$	94.4(2)	90(2)	90(2)	90(1)
N$_{tac}$−M−N$_{tac}$	83.0(1)	90.4(8)	90.0(6)	91(1)
X−Cu−O				96(2)

[a] M = Cr, Co; M′ = Ni, Cu; X indicates a C or N atom in a cyanide ligand; N$_{tac}$ indicates a N atom in a Me₃tacn or tach ligand. Distances are given in angstroms and angles are given in degrees for Me₃tacn, [(Me₃tacn)₈Cr₈Ni₆(CN)₂₄]Br₁₂·45H₂O;[9b] **12·6H₂O**, [(tach)₈Cr₈Ni₆(CN)₂₄]-Br₁₂·36H₂O; **13·11H₂O**, [(tach)₈Cr₈Ni₆(CN)₂₄⊃THF]Br₁₂·41H₂O; and **14**, [(tach)₈(H₂O)₆Cu₆Co₈(CN)₂₄⊃THF]Br₁₂·29H₂O.

noticeable in the two different Cr···Cr edge separations, as well as in the two distinct types of Cr−N−C angles: one significantly bent and the other essentially linear. The latter observation suggests that the distortion may originate from hydrogen-bonding interactions between solvate water molecules and the nitrogen ends of the six bent cyanide bridges [Cr(2)−N(3)−C(3) and its equivalents] situated around the waist of the cluster. Indeed, although there is considerable disorder among the solvate water molecules in the structure, the closest N···O contacts of 2.86 Å are found for these particular cyanide ligands. The next closest N···O contacts of this type are at a separation of 3.01 Å.

The tightly connected metal−cyanide cage of the [(tach)₈Cr₈Ni₆(CN)₂₄]¹²⁺ cluster encloses a sizable central cavity. Based on the trans-Ni···Ni distance of 8.994 Å and the estimated van der Waals radius of a nickel atom,[31] the minimum diameter of this cavity is approximately 5.2 Å. With a total volume close to the 284 Å³ interior capacity of [(Me₃-tacn)₈Cr₈Ni₆(CN)₂₄]¹²⁺,[9b] it differs slightly in overall shape as a result of the aforementioned trigonal compression. Most importantly, however, passage in and out of the cavity in [(tach)₈Cr₈Ni₆(CN)₂₄]¹²⁺ is not restricted by substituents on the outer capping ligands. As illustrated by the space-filling model in Figure 6, the less-encumbering tach ligands provide ready access to openings in the metal−cyanide cage. Due to the trigonal compression, two types of Cr₂Ni₂(CN)₄ windows are available: one with a minimum diameter of 1.4 Å (shown at the fore in the space-filling model), and another with a minimum diameter of 1.2 Å.[31] Note that both of these openings are slightly smaller than those present in the [(tach)₄(H₂O)₁₂M′₄M₄(CN)₁₂]⁸⁺ clusters discussed above, owing to the more bent cyanide bridges required in forming the face-centered cubic cage. Despite the open access, as crystallized by evaporation of an aqueous solution, no guest

water molecules are apparent inside the cavity of the [(tach)₈Cr₈Ni₆(CN)₂₄]¹²⁺ cluster. This contention is supported by the crystal structure of **12·6H₂O**, where no appreciable electron density is observed within the cluster cavity, and electrospray mass spectra of the compound, which display no peaks corresponding to the intact cluster plus water molecules. Here again, the absence of guest water molecules is attributed to the hydrophobic character of the cage interior and the availability of openings through which a guest molecule might escape.[37]

In distinct contrast with its Me₃tacn-capped analogue, the [(tach)₈Cr₈Ni₆(CN)₂₄]¹²⁺ cluster is amenable to host−guest chemistry. Initial experiments testing for guest inclusion were performed by electrospray mass spectrometry. An aqueous solution of compound **12** was charged with 10 molar equiv of THF and allowed to stand at room temperature. Aliquots of this solution were then extracted at intervals and injected directly into the mass spectrometer. Figure 7 shows the resulting positive ion spectra obtained under identical instrument conditions for aliquots withdrawn 5 min, 5 h, and 24 h after mixing. After just 5 min, the spectrum shows only minor differences from that observed in the absence of THF, wherein peaks corresponding to {[(tach)₈Cr₈Ni₆(CN)₂₄]Br₉₋ₙ}ⁿ⁺ (n = 3, 4, 5) are prominent. Upon further standing, however, new peaks corresponding to these compositions plus one THF molecule gradually emerge. After approximately 3 days, the spectra show no additional changes; evidence for association of more than one THF molecule never arises. Analogous experiments indicate uptake of several related molecules, including furan, tetrahydrothiophene, and 1,4-dioxane, but, interestingly, not 2-methylfuran.[38]

While these mass spectrometry experiments reveal a definite association between the [(tach)₈Cr₈Ni₆(CN)₂₄]¹²⁺ cluster and one molecule of THF, they do not prove that THF is included within the confines of the cluster cavity. However, confirmation of its encapsulation was provided through X-ray analysis of crystals of [(tach)₈Cr₈Ni₆(CN)₂₄⊃-THF]Br₁₂·41H₂O (**13·11H₂O**) grown by diffusing THF into a concentrated solution of **12**. The resulting structure features a THF molecule disordered over two equivalent orientations (one of which is depicted in Figure 8) in the center of the metal−cyanide cage. The guest molecule is suspended within the cavity and has no particularly close contacts with the atoms of the cage framework—the dashed line corresponds to a very long Ni···O contact of 3.43(6) Å and is intended more as a guide to the eye than indication of a bonding interaction. Interestingly, the metal−cyanide cage itself is essentially congruent with that observed for the empty cluster in **12·6H₂O** (see Table 6), despite the differing structure types. The mechanism whereby THF enters the cluster cavity is not yet clear; however, in view of the dimensions of a THF molecule relative to the cage openings, it is not necessarily the case that the process involves breaking Cr−N or Ni−C bonds. Tentative support for this

(37) We note, however, that despite the more hindered exitways of the fully formed cages, no guest water molecules are evident inside the [(Me₃tacn)₈M₈Ni₆(CN)₂₄]¹²⁺ (M = Cr, Mo) clusters.[9b,e]
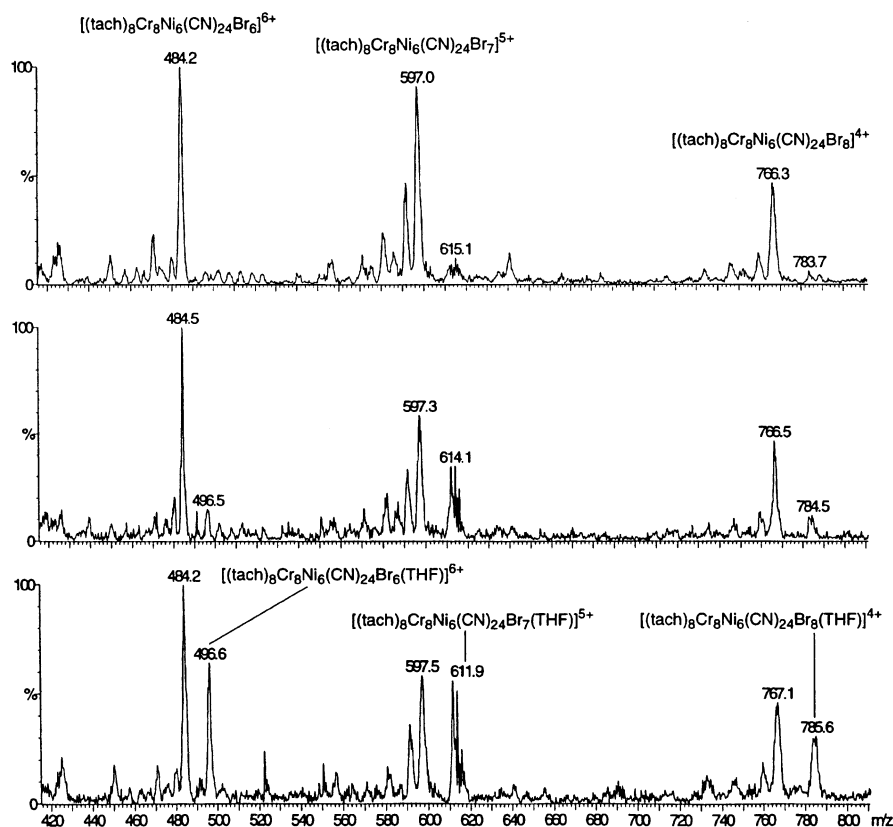(38) A. G. Hee and J. R. Long, work in progress.

Figure 7. Portion of the electrospray mass spectrum of a 0.5 mM aqueous solution of compound **12** charged with 10 equiv of THF. The upper, middle, and lower spectra correspond to samples of the solution extracted 5 min, 5 h, and 24 h after mixing, respectively. A comparison of observed and simulated isotope patterns for the species at $m/z = 496.6$ is depicted in Figure S6 of the Supporting Information.
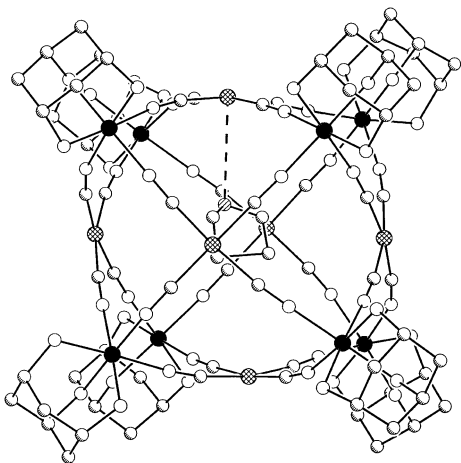

Figure 8. Structure of the face-centered cubic $[(tach)_8Cr_8Ni_6(CN)_{24}\supset\text{-}THF]^{12+}$ cluster in **13**·11H$_2$O. Black, crosshatched, shaded, white, and hatched spheres represent Cr, Ni, C, N, and O atoms, respectively; H atoms are omitted for clarity. The cluster resides on a crystallographic 2-fold rotation axis, which bisects the line connecting the leftmost and foremost Ni atoms. Accordingly, the guest THF molecule is disordered over two possible orientations, only one of which is depicted.

not being the case is found in the observation that THF is not encapsulated by $[(Me_3tacn)_8Cr_8Ni_6(CN)_{24}]^{12+}$ under similar conditions. Additional support may be inferred from the fact that 2-methylfuran should readily fit inside the cluster cavity but is not absorbed. More detailed experiments probing the kinetics and selectivity of the inclusion process are currently underway.[38]

As an apparent result of their confinement, the THF molecules are only reluctantly liberated from solid samples of **13**. This is evident in comparing the thermogravimetric analyses of compounds **12** and **13** (see Figure S7 in the Supporting Information). Both solids are completely desolvated by approximately 150 °C and begin to decompose at temperatures above 230 °C. However, while the loss of solvent from **12**, which contains no THF, is smooth and virtually without steps, the loss of solvent from **13** shows a minor hitch at 50 °C, followed by a broad hump that extends to approximately 140 °C. The mass difference between the two curves in the region from 80 to 140 °C is roughly consistent with retention of 1 equiv of THF per guest-containing cluster in the latter compound.

Numerous efforts were made to substitute odd-electron metal ions such as Co^{II} or Cu^{II} for the diamagnetic Ni^{II} centers in the $[(tach)_8Cr_8Ni_6(CN)_{24}]^{12+}$ cluster. Owing to its greater ease of preparation, many test reactions were carried out employing $[(tach)Co(CN)_3]$ in place of $[(tach)Cr(CN)_3]$. Whereas reactions between $[(tach)Co(CN)_3]$ and $[Co(H_2O)_6]^{2+}$ in aqueous solution were found to yield either cubic $[(tach)_4(H_2O)_{12}Co_8(CN)_{12}]^{8+}$ clusters or the two-dimensional $[(tach)(H_2O)_3Co_2(CN)_3]^{2+}$ framework described below, related reactions involving $[Cu(H_2O)_6]^{2+}$ succeeded in forming a face-centered cubic cluster. However, contrary to the situation with the chromium−nickel species, its formation was observed *only* upon crystallization from
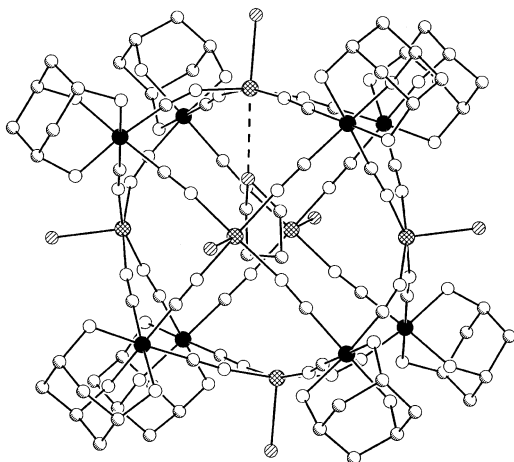
Figure 9. Structure of the face-centered cubic $[(tach)_8(H_2O)_6Cu_6Co_8-(CN)_{24} \supset THF]^{12+}$ cluster in **14**. Black, crosshatched, shaded, white, and hatched spheres represent Co, Cu, C, N, and O atoms, respectively; H atoms are omitted for clarity. The cluster resides on a $\bar{3}$ symmetry site in the crystal, with the 3-fold rotation axis penetrating the lower left front and upper right rear Co atoms. Accordingly, the guest THF molecule is disordered over six possible orientations, only one of which is depicted.

solutions containing THF, suggesting that THF acts as a templating agent.

X-ray analysis of a single crystal of $[(tach)_8(H_2O)_6Cu_6-Co_8(CN)_{24} \supset THF]Br_{12} \cdot 29H_2O$ (**14**) revealed the THF-containing cluster displayed in Figure 9. Comparison of its structure with that of $[(tach)_8Cr_8Ni_6(CN)_{24} \supset THF]^{12+}$ (see Figure 8 and Table 6) reveals several important differences. First, the cyanide ligands all maintain a $Co^{III}-C-N-Cu^{II}$ bridging arrangement, indicating that linkage isomerization is not involved in formation of the Cu_6Co_8 cluster. Accordingly, the Cu^{II} centers adopt a square pyramidal geometry, with water molecules providing the apical ligands. As a further consequence of this bridging arrangement, the distortion in the cluster cage—which again takes the form of a compression along a body diagonal of the cube—is accomplished through a more significant bending of the cyanide bridges at six of the face-centering metal sites instead of six of the corner metal sites. Finally, with a $Cu\cdots O$ distance of 2.82(3) Å, the encapsulated THF molecule in **14** apparently forms a stronger interaction with a face-centering metal ion of the cage.

Although the $[(tach)_8(H_2O)_6Cu_6Co_8(CN)_{24} \supset THF]^{12+}$ cluster contains paramagnetic metal ions in its face-centering positions, the Co^{III} ions at the corner sites are of course diamagnetic. Consequently, the magnetic behavior of **14** is consistent with six noninteracting Cu^{II} centers, each with a spin of $S = \frac{1}{2}$. Attempts to substitute Cr^{III} or Fe^{III} for Co^{III} in this cluster are ongoing; however, at least in the former instance, results thus far suggest a rapid loss of cyanide ligands to the softer Cu^{II} ions.

Extended Solid Frameworks. The cubic $[(tach)_4-(H_2O)_{12}M'_4M_4(CN)_{12}]^{8+}$ clusters described above are constructed of a 1:1 combination of $[(tach)M(CN)_3]$ complexes and fac-$[M'(H_2O)_3]^{2+}$ units. Interestingly, in the case of M = M' = Co, this structure type is frequently rejected in favor of an isomeric framework incorporating mer-$[Co(H_2O)_3]^{2+}$ units. Crystals of $[(tach)(H_2O)_3Co_2(CN)_3]Br_2 \cdot 5.5H_2O$ (**15**),

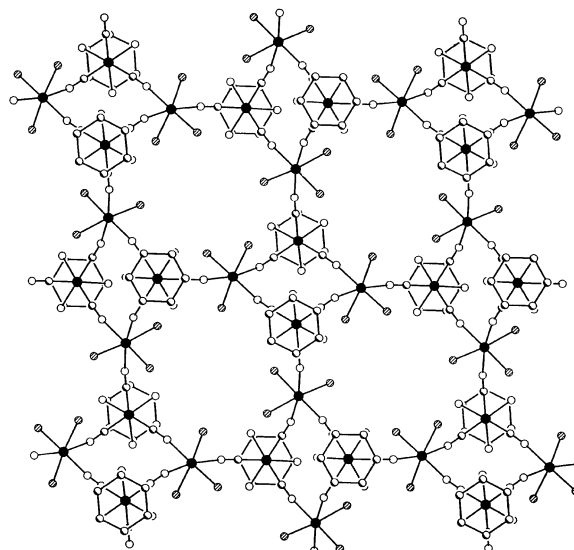**Figure 10.** Portion of a $[(tach)(H_2O)_3Co_2(CN)_3]^{2+}$ sheet in the structure of **15**. Black, shaded, white, and hatched spheres represent Co, C, N, and O atoms, respectively; H atoms are omitted for clarity. Crystallographic inversion centers reside in the middle of the squares and octagons that comprise the two-dimensional net. Selected interatomic distances (angstroms) and angles (degrees): Co−C 1.88(1), Co−N$_{tach}$ 1.987(5), Co−N$_{CN}$ 2.097(3), Co−O 2.10(4), C−N$_{CN}$ 1.151(4), Co⋯Co 5.11(2), Co−C−N$_{CN}$ 177(1), Co−N$_{CN}$−C 171(3), C−Co−C 87.1(9), C−Co−N$_{tach}$ 91(1), N$_{tach}$−Co−N$_{tach}$ 91(1), N$_{CN}$−Co−N$_{CN}$ 94(4), N$_{CN}$−Co−O 88(3), O−Co−O 92.15-(7).

formed by evaporation of an aqueous solution of $[(tach)Co-(CN)_3]$ and $CoBr_2$, are distinguishable from those of cube-containing **9** by their orange color. X-ray analysis of one such crystal revealed the nonplanar two-dimensional framework depicted in Figure 10. Here, $Co_4(CN)_4$ squares similar to those composing the faces of $[(tach)_4(H_2O)_{12}Co_8(CN)_{12}]^{8+}$ are corner-linked via cyanide to form a net containing holes based on octagonal $Co_8(CN)_{12}$ rings. These nets stack on top of each other, such that the $Co_4(CN)_4$ squares are centered over and under the $Co_8(CN)_{12}$ octagons in neighboring layers. To our knowledge, this structure is without precedent in metal−cyanide chemistry. The most notable difference between the metric parameters listed in the Figure 10 caption and those for the discrete cube isomer (see Table 5) lies in which end of the cyanide bridges is most bent. Analogous reactions utilizing $[(tach)Fe(CN)_3]$ afford the isostructural compound $[(tach)(H_2O)_3CoFe(CN)_3]Br_2 \cdot 5.5H_2O$, which potentially could have interesting photomagnetic properties.[4]

Ultimately, we seek methods for assembling molecular clusters capable of supporting extremely high-spin ground states. Toward that end, we have attempted numerous reactions of the following type, intended to produce edge-bridged cubic clusters:

$$8[(tach)M(CN)_3] + 12[(cyclam)M'(H_2O)_2]^{n+} \rightarrow$$
$$[(tach)_8(cyclam)_{12}M'_{12}M_8(CN)_{24}]^{12n+} \quad (6)$$
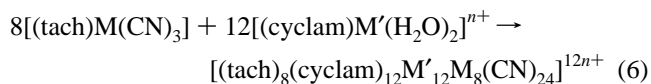
With an appropriate combination of metal centers, record spin states climbing as high $S = 26$ should be feasible for this geometry.[39] Related reactions employing $[(Me_3tacn)M-(CN)_3]$ (M = Cr, Mo) corner units were previously found to produce primarily linear $[(Me_3tacn)_2(cyclam)M'M_2(CN)_6]^{2+}$
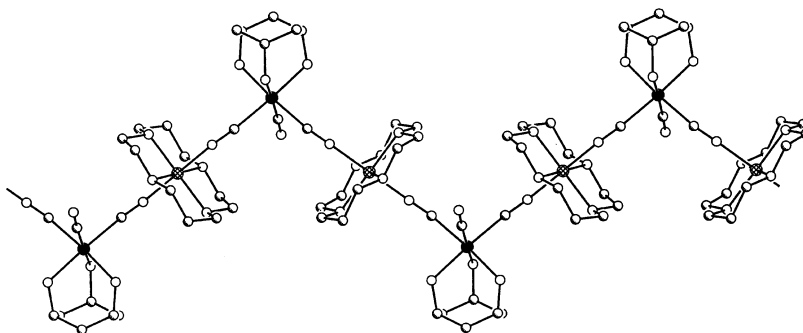
Figure 11. Portion of a one-dimensional [(tach)(cyclam)NiCr(CN)$_3$]$^{2+}$ chain in the structure of **16**·H$_2$O; H atoms are omitted for clarity. Black, crosshatched, shaded, and white spheres represent Cr, Ni, C, and N atoms, respectively. Crystallographic inversion centers are located at the Ni atoms running along the middle of the chain.

clusters or one-dimensional chains of formula [(Me$_3$tacn)-(cyclam)M′M(CN)$_3$]$^{2+}$.[9b,e] Use of the more compact tach ligand was expected to eliminate any steric conflict between Me$_3$tacn and cyclam that might be interfering with cluster assembly. Furthermore, it was thought that N−H···O···H−N hydrogen-bonding interactions between tach, water, and cyclam could potentially help stabilize an edge-bridged cubic structure, similar to the way in which hydrogen bonding supports formation of the cubic [(tach)$_4$(H$_2$O)$_{12}$M′$_4$M$_4$-(CN)$_{12}$]$^{8+}$ clusters. Thus far, however, reactions of type 6 have instead led only to crystalline products containing extended one- or two-dimensional frameworks.

Evaporation of an aqueous solution containing [(tach)Cr-(CN)$_3$], Ni(cyclam)I$_2$, and excess KPF$_6$ affords yellow plate-shaped crystals of [(tach)(cyclam)NiCr(CN)$_3$](PF$_6$)$_2$·2H$_2$O (**16**·H$_2$O).[40] Figure 11 displays the structure of the one-dimensional zigzag chains of alternating [(tach)Cr(CN)$_3$] and [(cyclam)Ni]$^{2+}$ units residing therein. Each chromium center has one terminal cyanide ligand, and these are arranged in an anti conformation with respect to each other along the chain. An isotypic structure occurs in [(Me$_3$tacn)(cyclam)-NiMo(CN)$_3$]I$_2$·4H$_2$O,[8e] and related chains containing [M(CN)$_6$]$^{3−}$ (M = Cr, Fe, Co) units in place of [(tach)Cr-(CN)$_3$] have also been reported.[41] An analogous reaction generates the isostructural compound [(tach)(cyclam)NiFe-(CN)$_3$](PF$_6$)$_2$·H$_2$O; however, owing to previous characterization of related chains,[41] the magnetic properties were not studied for either compound.

In the absence of KPF$_6$, the reaction between [(tach)Cr-(CN)$_3$] and [Ni(cyclam)I$_2$] in aqueous solution produces [(tach)$_2$(cyclam)$_3$Ni$_3$Cr$_2$(CN)$_6$]I$_2$ (**17**). Although the formulation of this compound is consistent with that of the intended edge-bridged cubic cluster, its crystal structure instead contains the isomeric two-dimensional framework shown in Figure 12. Here, [(tach)Cr(CN)$_3$] complexes are connected to [Ni(cyclam)]$^{2+}$ units through all three cyanide ligands, creating a hexagonal net comprised of nonplanar Ni$_6$Cr$_6$-

(CN)$_{12}$ rings in a chair conformation. These nets stack such that the tach ligands project into the holes created by the Ni$_6$Cr$_6$(CN)$_{12}$ rings in neighboring layers. Interestingly, the chains in **16**·H$_2$O represent one-dimensional fragments of the sheets in **17**, although a comparison of the metric parameters for two structures (see Table 7) reveals substantial differences in the C−Cr−C and Ni−N$_{CN}$−C angles. Reactions performed with [Cu(cyclam)](NO$_3$)$_2$ led to a series of isostructural compounds, [(tach)$_2$(cyclam)$_3$Cu$_3$M$_2$(CN)$_6$]$_2$-(NO$_3$)$_2$ [M = Cr (**18**), Fe, Co], all featuring analogous two-dimensional sheets. As evident from comparing the mean M′−N$_{CN}$ distances listed in Table 7, the metal−cyanide framework of **18** is more weakly connected than that of **17**. Numerous compounds with equivalent hexagonal sheets incorporating [M(CN)$_6$]$^{3−}$ (M = Cr, Fe, Co) units or other related complexes have been reported previously.[19a,42] Potentially, the judicious choice of a templating counteranion could still permit the successful implementation of reaction 6.

The magnetic properties of **17** are suggestive of meta-magnetic behavior similar to that observed in the closely related compounds [Ni(cyclam)]$_3$[Cr(CN)$_6$]$_2$·20H$_2$O and [NiL]$_3$-[Cr(CN)$_6$]$_2$·18H$_2$O (where L = 3,10-bis(2-hydroxyethyl)-1,3,5,8,10,12-hexaazacyclotetradecane).[42a,f] In an applied field of 1000 G, the value of $\chi_M T$ for **17** increases monotonically as the temperature is lowered, achieving a maximum of 365.44 cm^3·K/mol at 10 K and then decreasing to 230.24 cm^3·K/mol at 5 K (see Figure S8 in the Supporting Information). The monotonic rise is consistent with the expected[11] ferromagnetic coupling between the cyanide-bridged Cr^{III} and Ni^{II} centers. The maximum value of $\chi_M T$ is much higher than observed in either of the compounds containing [Cr(CN)$_6$]$^{3−}$, which suggests the presence of long-range ordering of the intralayer spins. However, as in the

(39) For example, with M = Fe^{III} and M′ = Mn^{II}, antiferromagnetic coupling[11] between neighboring metal centers would be expected to give rise to an S = 26 ground state.

(40) Note that, as specified in the Experimental Section, the source of [(tach)Cr(CN)$_3$] and Ni(cyclam)I$_2$ in this reaction was compound **17**, which dissociates in aqueous solution.

(41) Ohba, M.; Usuki, N.; Fukita, N.; Okawa, H. *Inorg. Chem.* **1998**, *37*, 3349.

(42) (a) Ferlay, S.; Mallah, T.; Vaissermann, J.; Bartolomé, F.; Veillet, P.; Verdaguer, M. *Chem. Commun.* **1996**, 2481. (b) Kou, H.-Z.; Gao, S.; Bu, W.-M.; Liao, D.-Z.; Ma, B.-Q.; Jiang, Z.-H.; Yan, S.-P.; Fan, Y.-G.; Wang, G.-L. *J. Chem. Soc., Dalton Trans.* **1999**, 2477. (c) Colacio, E.; Domínguez-Vera, J. M.; Ghazi, M.; Kivekäs, R.; Lloret, F.; Moreno, J. M.; Stoeckli-Evans, H. *Chem. Commun.* **1999**, 987. (d) Kou, H.-Z.; Bu, W.-M.; Gao, S.; Liao, D.-Z.; Ma, B.-Q.; Jiang, Z.-H.; Yan, S.-P.; Fan, Y.-G.; Wang, G.-L. *J. Chem. Soc., Dalton Trans.* **2000**, 2996. (e) Kou, H.-Z.; Gao, S.; Ma, B.-Q.; Liao, D.-Z. *J. Chem. Soc., Dalton Trans.* **2000**, 2996. (f) Xiang, H.; Gao, S.; Lu, T.-B.; Luck, R. L.; Mao, Z.-W.; Chen, X.-M.; Ji, L.-N. *New J. Chem.* **2001**, *25*, 875. (g) Shen, Z.; Zuo, J.-L.; Shi, F.-N.; Xu, Y.; Song, Y.; You, X.-Z. *Trans. Met. Chem.* **2001**, *26*, 345.
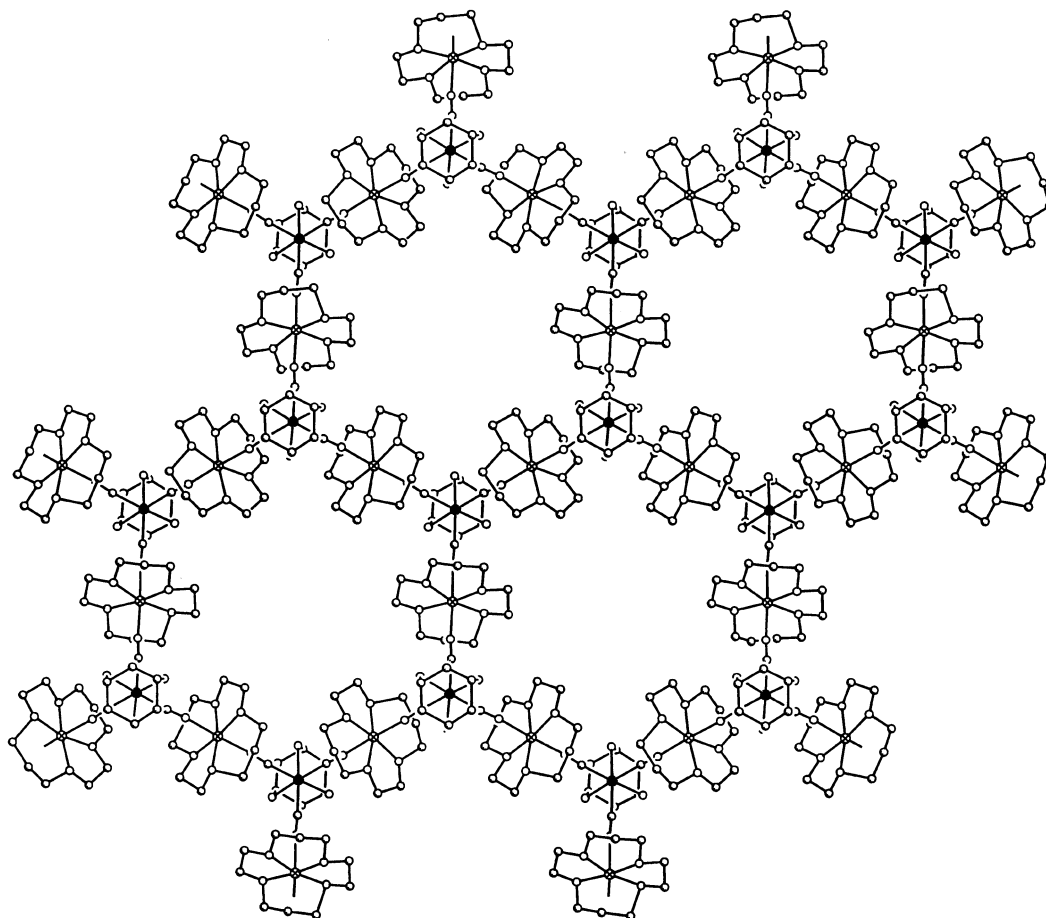
Figure 12. Portion of a two-dimensional [(tach)$_2$(cyclam)$_3$Ni$_3$Cr$_2$(CN)$_6$]$^{6+}$ sheet in the structure of **17**. Black, crosshatched, shaded, and white spheres represent Cr, Ni, C, and N atoms, respectively. For clarity, H atoms are omitted and only one of the orientations of the disordered cyclam ligands is depicted. The Cr atoms reside on 3-fold rotation axes, while Ni atoms are positioned on perpendicular 2-fold rotation axes.

Table 7. Selected Mean Interatomic Distances and Angles for the One-Dimensional Chains and Two-Dimensional Sheets in the Structures of **16·H$_2$O**, **17**, and **18**[a]

	16·H$_2$O	17	18
Cr–C	2.069(6)	2.102(8)	2.072(2)
M′–N$_{CN}$	2.125	2.17(6)	2.371(2)
C–N$_{CN}$	1.148(2)	1.144(9)	1.149(3)
Cr–N	2.076(2)	2.089(7)	2.076(2)
M′–N$_{cyclam}$	2.08(2)	2.08(5)	2.033(4)
C–Cr–C	84.7(2)	91.4(3)	86.48(8)
	96.5(3)		
Cr–C–N$_{CN}$	169(3)	173(1)	175.7(2)
N$_{CN}$–M′–N$_{CN}$	180	177.4(9)	180
M′–N$_{CN}$–C	160.2(5)	175(2)	161.6(2)
N–Cr–C	91(3)	90(2)	92(1)
N–Cr–N	89(2)	89.4(3)	89.28(7)
N$_{cyclam}$–M′–N$_{CN}$	90(3)	90(4)	89.4(8)
N$_{cyclam}$–M′–N$_{cyclam}$	84.7	90(11)[b]	85.45(7)
	95.3		94.55(7)

[a] M′ = Ni, Cu; N$_{CN}$ and N$_{cyclam}$ indicate N atoms in cyanide and cyclam ligands, respectively. Distances are given in angstroms and angles are given in degrees for **16·H$_2$O**, [(tach)(cyclam)NiCr(CN)$_3$](PF$_6$)$_2$·2H$_2$O; **17**, [(tach)$_2$(cyclam)$_3$Ni$_3$Cr$_2$(CN)$_6$]I$_6$; and **18**, [(tach)$_2$(cyclam)$_3$Cu$_3$Cr$_2$(CN)$_6$](NO$_3$)$_6$·XH$_2$O. [b] The cyclam ligands in this structure are disordered.

case of these two other compounds,[42a,f] the subsequent downturn in $\chi_M T$ is attributed to antiferromagnetic coupling between layers. Potentially, the greater maximum value of $\chi_M T$ observed for **17** is a consequence of weaker interlayer exchange interactions. This possibility is supported by the

significantly longer distances of 9.619, 9.758, and 9.638 Å found for the nearest interlayer Cr···Cr, Cr···Ni, and Ni···Ni contacts.

Outlook

The foregoing results demonstrate the utility of tach as a capping ligand in generating high-nuclearity metal–cyanide clusters. In particular, the compact nature of the ligand provides open access to the cavities defined by the metal–cyanide cages of cubic and face-centered cubic clusters. These new molecular species present a unique opportunity for studying inclusion phenomena within relatively rigid cage constructs. Additionally, the ability to substitute various metal ions into the structure types disclosed herein should enable adjustment of the magnetic properties to give higher-spin ground states and, potentially, the magnetic anisotropy required for a single-molecule magnet. Toward the latter end, the wider N–M–N bite angles sustained by tach relative to tacn or Me$_3$tacn may be of advantage in maintaining an octahedral coordination geometry for complexes of second- and third-row transition metal ions (which generally exhibit greater spin–orbit coupling but also a larger radius).[9e] Ultimately, we hope that the reaction chemistry introduced here will prove of value in assembling clusters for future use in information storage and/or spin-based molecular electronics devices.

Supporting Information Available: Depictions of the structure of **3**·0.6MeCN and the hydrogen-bonding interactions in the structure of **11**, plots of the magnetic susceptibility data for compounds **5**, **6**, and **17**, the EPR spectrum of **6**, observed and simulated isotope patterns for a peak in the mass spectrum of **13**, thermogravimetric analyses of **12** and **13** (PDF) and X-ray structural information for the compounds listed in Tables 1−3, including tables of crystal and refinement data, atomic positional and thermal parameters, and interatomic distances and angles (CIF). This material is available free of charge via the Internet at http://pubs.acs.org.

IC026065F